QUANTIFYING SHORELINE CHANGE AT THREE DIVERSE COASTAL GEOMORPHOLOGIES ON HAWAIʻI ISLAND

A THESIS SUBMITTED TO THE GRADUATE DIVISION OF THE UNIVERSITY OF HAWAIʻI AT HILO IN PARTIAL FULFILLMENT OF THE REQUIREMENTS FOR THE DEGREE OF

MASTER OF SCIENCE

IN

TROPICAL CONSERVATION BIOLOGY AND ENVIRONMENTAL SCIENCE

JUNE 2018

By: Rose Sierra Hart

Thesis Committee:

Ryan Perroy, Chairperson

Charles Fletcher

Steven Colbert

Bethany Morrison

Keywords: Small unmanned aerial systems, coastal vulnerability, erosion, sea level rise, subsidence, coastal zone management

ACKNOWLEDGEMENTS

I would like to gratefully acknowledge funding support and collaboration from the United States Geological Survey (USGS) via the Pacific Islands Climate Science Center through Cooperative Agreement G12AC00003, without which this project would not be possible.

I would like to give very special thanks to my graduate committee, who have taught, humbled, encouraged, and inspired me as I pursued my master's degree. Dr. Ryan Perroy has been an incredible mentor throughout my undergraduate and graduate careers, and I could not have completed my research without his unwavering support, careful advising, unmatched patience, and very dry humor. Dr. Charles (Chip) Fletcher and his research on coastal change in Hawaiʻi has been a huge inspiration for me; Chip's knowledge greatly informed methodologies and discussion within my thesis. Dr. Steven Colbert taught me almost everything I know about coastal geology and was instrumental in helping me interpret my data. Bethany Morrison, and her aspirations for the Hawaiʻi County Planning Department, motivated my thesis and I am very grateful for her engaging me at the interface of science and policy.

I would like thank past and present colleagues, who I am fortunate to call friends, at the University of Hawaiʻi at Hilo Spatial Data Analysis and Visualization Lab: Nathan Stephenson, Kelly Goodale, Harrison Andina, David Russel, Timothy (Timo) Sullivan, and James (Kimo) Melcher. These individuals provided incredible support in the field and in the lab.

I would like to thank Matthew Barbee, Dr. Tiffany Anderson, Ayesha Genz, Matthew Lucas, and Dr. Robert Thieler, who let me pick their brains on many accounts.

I would like to thank Hawaiʻi County Planning Department, Hawaiʻi State Parks, Hāpuna Beach Prince Hotel, and the Honoliʻi and Kapoho residents for allowing me to work within their communities.

Lastly, I would like to thank my friends and family for their comedic relief and moral support.

ABSTRACT

Hawai‘i Island's coastal communities are in a weak position for adapting to the impacts of sea-level rise (SLR), coastal erosion, and subsidence. Though bounded by nearly 430 km of ecologically, culturally, and economically important coastline, Hawai‘i Island has never had a comprehensive assessment, or systematic monitoring, of long-term and short-term shoreline change rates to inform local coastal zone management policies. Consequently, occurrences of unsustainable coastal development have resulted in significant impacts to property and nearshore resources. To better understand and manage coastal vulnerabilities, we quantified shoreline change from the mid-twentieth century to the present for three diverse geomorphic coastal settings on Hawai‘i Island. These sites are a calcareous beach (Hāpuna State Beach Park), a sea cliff (Honoli‘i Beach Park), and a subsiding coastal lava field (Kapoho/Hawaiian Vacation Land). In order to quantify change, we produced shoreline position data using historic aerial photographs and three-dimensional datasets derived from monthly small unmanned aerial system (sUAS) surveys collected over a 12 month period. These data were merged with SLR and subsidence projections using GIS to estimate and visualize current and future shoreline locations at our three sites. From our monthly survey data at Hāpuna Beach, we found the shoreline to be highly dynamic, exhibiting a mean intra-annual shoreline positional variation of 7.33 ± 2.29 m. We also found that Hāpuna Beach experiences long-term erosion (1969-2018) at a rate of -0.18 ± 0.17 m yr^{-1}. Along the Honoli‘i sea cliff, we quantified long-term erosion of -0.13 ± 0.26 m yr^{-1}, with a maximum retreat of 9.5 m between 1964 and 2018. Our analyses for Kapoho found that present-day extreme flooding events (i.e. king tides) already cause tidal inundation 60 m inland from the current mean higher high water mark. If SLR and subsidence rates persist as expected, the entire Kapoho study site will experience flooding within 25 years. Through this study we were able to quantify, for the first time, shoreline changes exhibited across Hawai‘i Island's diverse and dynamic coast. We also demonstrated the viability of sUAS as an effective tool for high resolution coastal monitoring. Our results provide insights to the chronic, seasonal, and episodic coastal processes that impact coastal communities and resources on Hawai‘i Island, and can help Hawai‘i County planners develop necessary adaptations to coastal management strategies.

TABLE OF CONTENTS

LIST OF TABLES

LIST OF FIGURES

CHAPTER 1. INTRODUCTION

Coastal and island communities worldwide are severely threatened by sea level rise and exacerbated effects from coastal erosion and subsidence. Impacts from these processes, including nuisance flooding, beach loss, cliff retreat, and infrastructure damage, are not trivial and will only amplify as human population and development pressures increase along the world's coasts (Neumann et al., 2015a; Neumann et al., 2015b). It is therefore necessary to research the combined effects of dynamic coastal processes to inform local coastal zone management policies, such as shoreline setbacks, and build community resiliency (Tribbia and Moser, 2008; Abbott, 2013).

Hawaiʻi, USA, is a remote archipelago in the middle of the Pacific Ocean, and is already experiencing the exacerbated consequences of sea level rise (SLR) and unsustainable coastal development. More than 20 km of Hawaiʻi's former coast has been completely lost to erosion, while urban regions like Honolulu regularly experience flooding due to seawater backwash into city storm drains during high tide (Romine and Fletcher 2013; Habel et al., 2017). Some of these impacts are the result of ambiguous coastal policies that have allowed hazardous coastal development and subsequently restricted natural and anthropogenic dynamic coastal processes (Dugan et al., 2010; Abbott, 2013). Concerted efforts have been focused on identifying, quantifying, and mitigating coastal vulnerabilities to the state's, and nation's, most valued biological, cultural, and economic resources (Neumann, 2015 (A); Sweet et al., 2017). One approach to mitigating future hazards is through the use of scientifically supported shoreline setbacks developed via collaboration of researchers, county planners and local policy makers.

In Hawaiʻi, the shoreline is broadly defined as the highest annual wash of the waves, with some exceptions for artificial structures that have augmented the shoreline. At the state level the shoreline setback is defined as an absolute minimum of twenty feet and an absolute maximum of forty feet from the designated shoreline (Hawaiʻi Revised Statutes §205A-43). However, HRS §205A-45 allows each county to establish setbacks greater than the state maximum. At the Hawaiʻi county level, which encompasses the entire island of Hawaiʻi, the shoreline setback is a minimum of forty feet for all lots, with some exceptions that allow for a twenty foot setback (Rule 11, Shoreline Setback of the Hawaiʻi County Planning Department Rules of Practice and

Procedure). These policies have been established without any research supporting that twenty or forty feet is a reasonable and safe setback. This is particularly problematic for Hawaiʻi Island, which has nearly 430 km of diverse coast including sea cliffs, sandy beaches, and low-lying lava fields. Further, shoreline adjacent lots are subject to various levels of zoning and development. Scientific support is needed for coastal zone management policies to effectively protect marine resources and the people who reside, work, and enjoy recreation along Hawaiʻi's treasured coastline. Maui and Kauaʻi Counties have used HRS-205A-45 to extend their shoreline setback boundaries based on best available science (Abbott, 2013; Romine and Fletcher 2013). However, scientific data describing shoreline change on Hawaiʻi Island is not available, motivating the topic of this thesis.

Here we quantify, for the first time, shoreline change at three diverse coastal geomorphologies that represent the diversity of Hawaiʻi Island's coast. Our study sites included a white sandy beach (Hāpuna State Beach Park), a sea cliff (Honoliʻi beach park), and a low-lying subsiding lava field (Kapoho/Vacation Estates). We used a combination of historic aerial imagery and imagery systematically acquired from a small unmanned aerial system (sUAS) to determine long-term (decadal) and short-term (monthly) shoreline change rates. The next three chapters describe the results from each study site and the fifth chapter discusses how our results can inform coastal zone management strategies for Hawaiʻi County and beyond.

CHAPTER 2. SHORELINE CHANGE AT HAPUNA STATE BEACH PARK

2.1. Introduction

2.1.1. Project Significance

Sandy beaches are important recreational, economic, cultural, and biological resources worldwide. Unfortunately, some of the world's most important beaches are being lost to coastal erosion and sea level rise. It is estimated that the United States has 4,300 km of severely eroding coastline, with 21 km of beach coast completely lost to erosion in Hawaiʻi (Houston, 2008; Romine and Fletcher, 2013). Scientists, engineers, local city managers and planners have worked together to mitigate beach loss by building groins, breakwaters, sea-walls, and replenishing the sand itself. These strategies, however, are costly, provide only a temporary solution, and often create unintended negative impacts (Landry et al., 2003; Romine and Fletcher, 2013; Brown et al., 2016). Some coastal communities have sought scientific support for creating policies that limit and remediate coastal development, rather than attempt to control coastal erosion and rising seas. For example, a study conducted in Yanchep, Australia, analyzed 34 years of data and reported a rate of -1.7m yr^{-1} of beach loss; those data have been useful for preventing hazardous coastal development along Western Australia's coasts (Gallop et al. 2015). This approach of integrating data to better inform local coastal zone management policies has also been tested and applied in the major counties of Hawaiʻi , specifically Maui, Oʻahu , and Kauaʻi (Romine and Fletcher, 2013).

Research on Oʻahu has quantified place-based erosion rates to estimate how economically important beaches will change in the future (Anderson et al., 2015; Habel et al., 2017), and extensive public outreach and education efforts by UH Mānoa SOEST researchers have begun to raise general awareness on this important issue. Furthermore, the counties of Maui and Kauaʻi have produced scientifically supported shoreline setback policies and community resiliency plans that incorporate coastal erosion rates (Maui Planning Commission, 2007; Abott, 2013; Council of the County of Kauaʻi, 2014). Despite these growing efforts across the state, there has been no study of long-term or short-term shoreline change for the County of Hawaiʻi. Although white sandy beaches are just one component of Hawaiʻi Island's diverse coast, they are important for recreation and tourism. Thus, it is important to expand upon methodologies from neighbor island studies to improve coastal monitoring strategies and identify any detrimental changes to Hawaiʻi County's beaches. One approach to improve shoreline monitoring strategies is through the adoption of small unmanned aerial systems (sUAS), which allow data acquisition on a shorter temporal scale compared to traditional historic image analyses.

2.1.2. Environment

Hāpuna State Beach Park (~10 ha), located on the northwest coast of Hawaiʻi Island (Figure 1), is the island's most popular white sandy beach. Hāpuna Beach is surrounded by lava rock and has two ephemeral streams that flow in at the north and south end of the beach during rare, heavy rain events (Fletcher et al., 2002; Bode and Jol, 2006). This coastal setting is exposed to west and northwest swell and Kona storms that can generate moderately high waves of 3m - 6 m, though waves are generally ~ 1m in height (Fletcher et al., 2002; Vitousek et al., 2009).

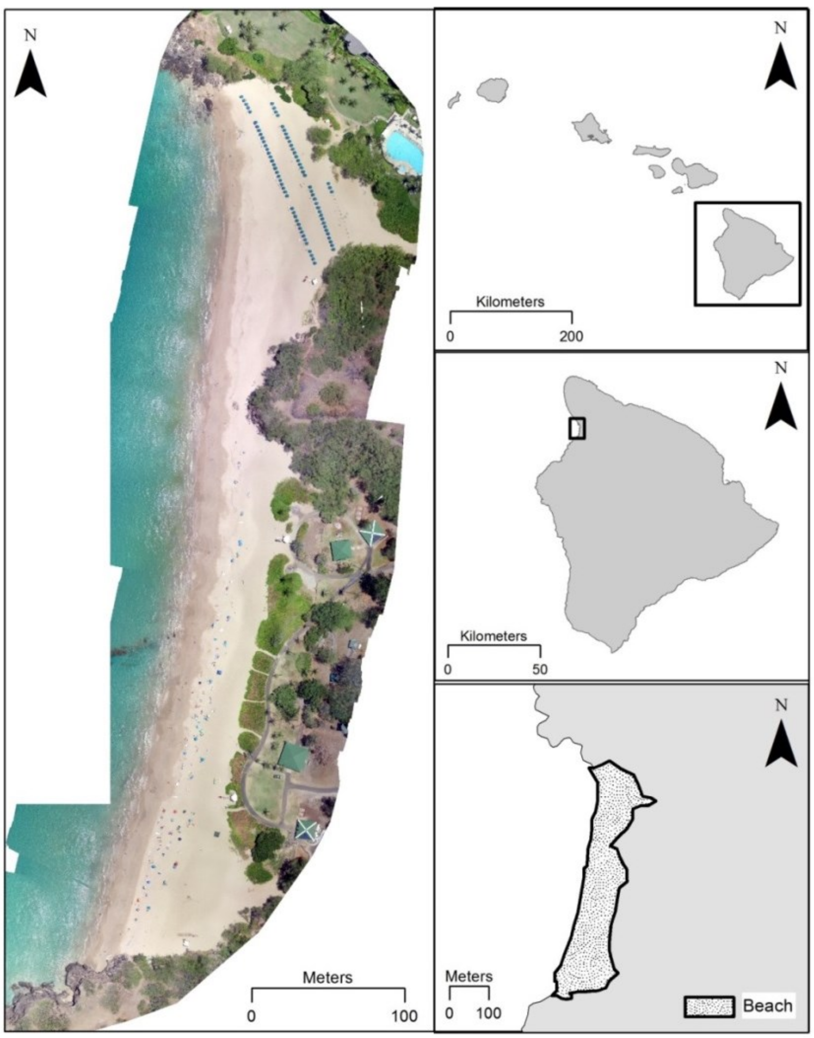

Figure 1. Map of Hāpuna State Beach Park. Top inset map shows the location of Hawaiʻi Island within the state; Middle inset highlights the region of Hawaii Island where Hāpuna Beach is located; and bottom inset identifies the extent of sandy beach. Left is a sUAS-derived orthophotomosaic of the site collected on 7/11/2017.

The development of walkways, pavilions, and a resort hotel along the beach began in the 1960s, and has created easy access for more visitors and locals to enjoy the beach (Bode and Jol, 2006). In a survey conducted for the Hāpuna Beach State Recreation Area Expansion Master Plan, Pederson Planning Consultants (1992) found that 75% of all shoreline and beach recreation along the Hāpuna-Puako coast occurred at Hāpuna Beach. In 2013, the Division of State Parks initiated a $5.00 entry fee for out of state visitors and $10.00-$40.00 for tour companies; these revenues have been used to support beach park maintenance and lifeguard services. It is possible, though, that coastal erosion and sea level rise could have dramatic consequences for the beach itself and those who depend on and use the beach in various capacities.

2.1.3. Objectives

The objectives for this study were to quantify long-term (decadal) and short-term (intra annual/monthly) shoreline change at Hāpuna State Beach Park and consider potential future vulnerability to SLR. We hypothesized that Hāpuna Beach has been subject to long-term erosion along the beach toe and could expect intensified seasonal beach fluctuations, or loss, if SLR continues as expected (Parris et al., 2012; Sweet et al., 2017). This chapter describes how we quantify long- and short-term shoreline change, potential future vulnerabilities to Hāpuna Beach, and how local planning can adapt to the potential changes.

2.2. Methods

2.2.1. Short-term shoreline change

In order to capture seasonal short-term seasonal and episodic erosive events, we used sUAS platforms to collect high-resolution imagery on a bi-monthly basis from January 2017 until January 2018 (Table 1). sUAS flight operations were conducted with a DJI Inspire 1 sUAS platform carrying a Zenmuse X3 camera, which had a 35 mm focal length and took RGB photographs with a 12-megapixel resolution. All sUAS flights were conducted in compliance with the Federal Aviation Administration (FAA) regulations (https://www.faa.gov/uas/media/RIN_2120-AJ60_Clean_Signed.pdf).

Table 1. sUAS surveys conducted for Hāpuna Beach. * Indicates failed flight mission that was not included in analysis.

Date	*Pictures Taken*	*Pixel Size (m)*	*RMSE (m)*
1/4/2017	275	0.02	0.05
3/1/2017	335	0.02	0.05
5/1/2017	234	0.02	0.04
7/11/2017	290	0.02	0.03
9/18/2017	344	0.02	0.03
*11/22/2017	385	0.02	0.14
12/5/2017	298	0.02	0.04
1/22/2018	299	0.02	0.03

sUAS flights were conducted at 45 m altitude during low tide, parallel to the shoreline, and images were taken with 75% overlap to render an orthophotomosaic of the site at ~ 0.02 m resolution (Goncalves and Henriques, 2015; Yoo and Oh, 2016; Casella et al., 2016) (Figure 2). A Trimble R8 differential GPS and Sokkia SCT6 total station were used to record ground control point (GCP) coordinates on both invariant (fixed) locations and variable features (i.e. beach sand) (Habel et al., 2016; Stephenson et al., 2017) (Figure 2). Invariant features included survey pins along the paved beach walkway and a rock outcropping towards the northern end of the beach. Variant features were white crosses, made out of perpendicular three-foot rebar sections covered in white duct tape, that were placed across the beach prior to each flight. Variant GCP coordinates were measured via total station, with typical errors on the order of 0.03 m. Having adequate GCPs within the area of interest is crucial for linking together each orthophotomosaic and generating reliable 3D models of changing natural surfaces (Goncalves and Henriques, 2015).

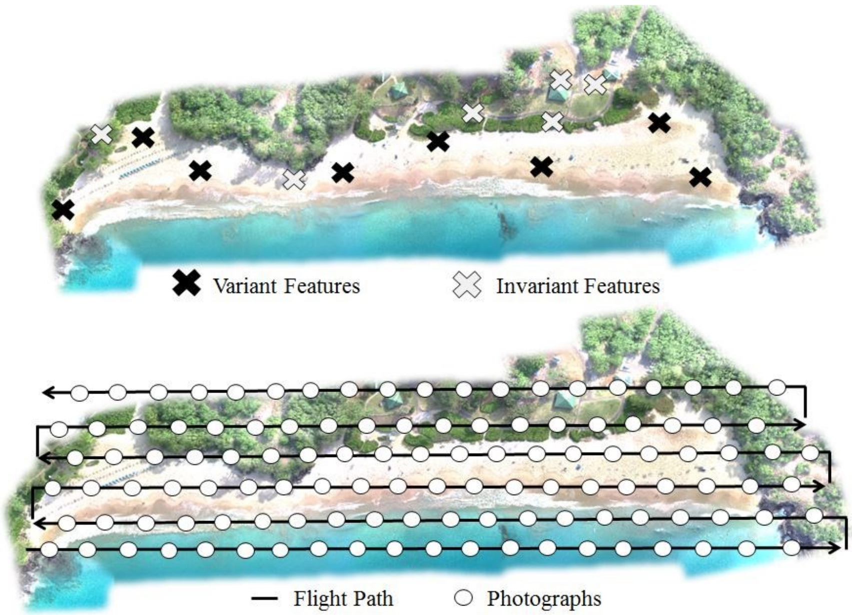

Figure 2. (Top) Ground control point distribution and (Bottom) sUAS flight path (black) and image acquisition (white dots).

Digital elevation models (DEMs) with 0.30 m pixel sizes were rendered from 3D data sets processed in Pix4D (Pix4D SA Switzerland) and LAStools (rapidlasso, 2015) (Figure 3). We first used Pix4D to process our sUAS-acquired imagery with our surveyed ground control points, which rendered a point cloud we could further process in LAStools. We use three distinct features in LAStools to produce a digital elevation model and thus remove features on the beach that do not represent the true ground. We first used "lasthin" to reduce point density to only the points with the lowest elevation in a 0.30 m grid. Second, we extracted bare earth data from the thinned point cloud using "lasground_new" with the "wilderness" filter, which identifies and removes small features (3 m step size) from the point cloud. Lasground_new creates two classifications: ground points (class = 2) and non-ground points (class = 1). Lastly, we process our classified point cloud, keeping only class two, and processing these data in "blast2DEM," to render a 0.30 m DEM.

Short-term coastal change was measured three ways using GIS: 1) we applied the raster calculator tool to subtract each DEM by the previous month's DEM, to identify regions of either sand erosion or accretion throughout the year; 2) we digitized shoreline vectors using the beach toe (i.e. low water position) for each dataset to measure the variation in shoreline position throughout the year; and 3) we measured the area of the beach using the mean low water position and the vegetation line as our beach area boundaries. All data were projected in WGS 83 for UTM Zone 5.

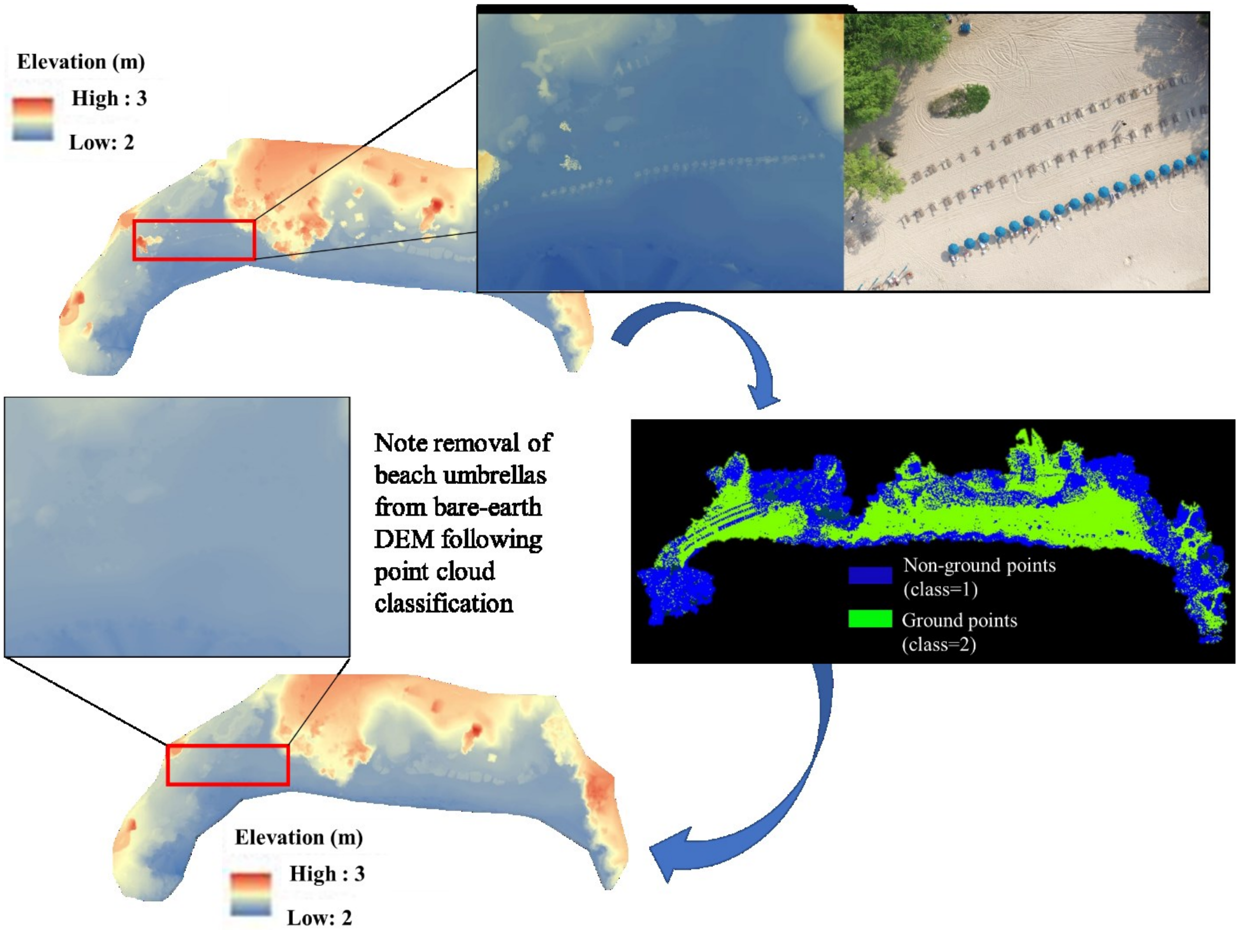

Figure 3. Results of filtering raw point cloud to produce a bare-earth DEM.

An initial root mean square error (RMSE) estimate of the 3D datasets was calculated in Pix4D Mapper Pro software, which estimates the error in the X, Y, and Z directions for all GCP locations. This error was computed to be ± 0.02 m on average for all datasets. We further determined the accuracy of our DEMs by conducting independent checks along permanent "control" features, as well as other random unmoving features, present in all datasets which should exhibit no change (Turner et al., 2016; Habel et al., 2016); these features included points along the paved beach path, water spigots, and cement grill stations (Figure 4). These control features were not included as GCPs for data/image processing. We measured the accuracy of our DEMs to be ± 0.05 m for all datasets by quantifying the standard deviation of these independent checks across each dataset and reporting the mean at the 95% confidence interval.

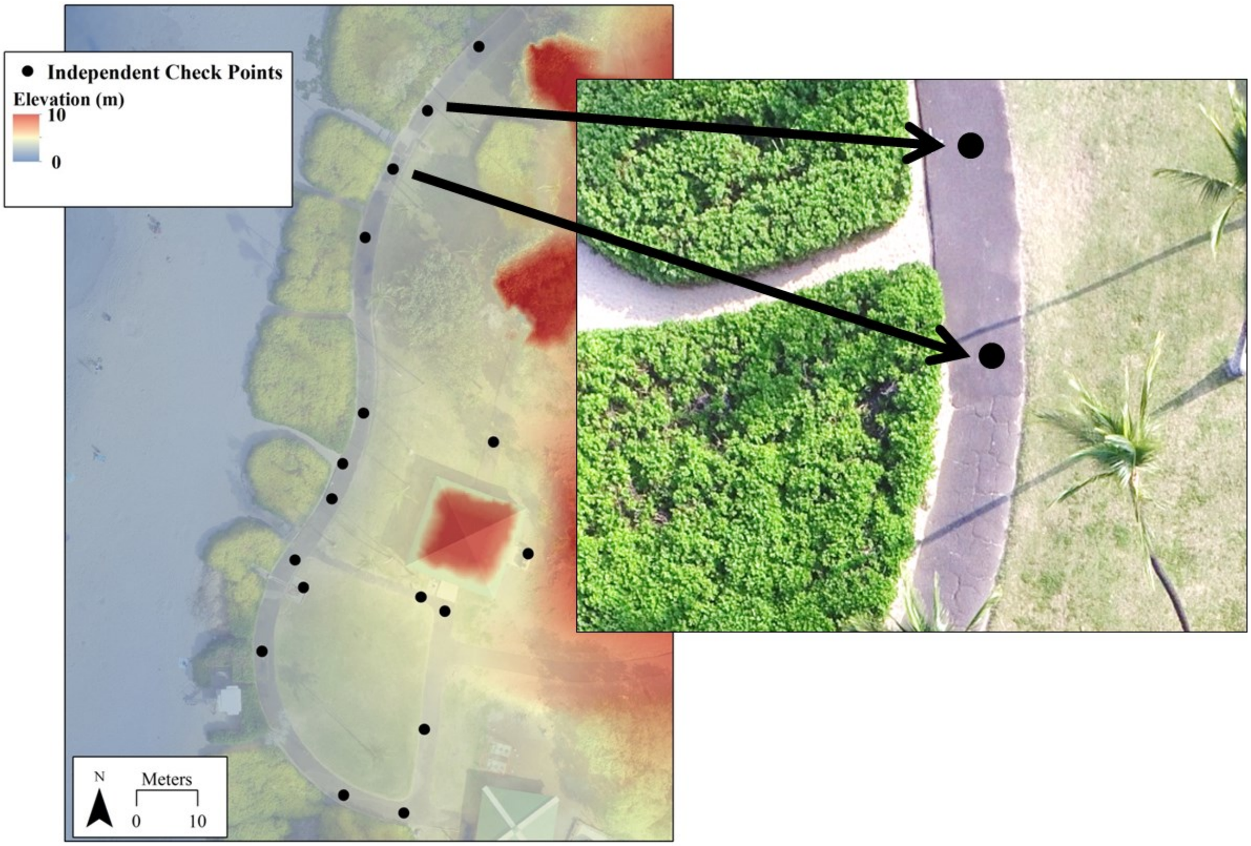

Figure 4. Example of independent, unmoving check points used to determine the accuracy of the DEMs.

2.2.2. Long-term shoreline change

2.2.2.1 Data acquisition

We gathered all available historic aerial photographs from Hawaiʻi County archives, the University of Hawaiʻi at Hilo Geography Department, and UH Mānoa Maps, Aerial Photographs, and GIS (MAGIS) program. We only selected nadir images that had a scale ≥ 1:25,000 and were in sharp focus (i.e. little to no blur due to motion or ambiguity from shadows). Based on these criteria, we gathered a total of 8 images (Table 2) that were scanned at a resolution between 720 and 1200 dpi. Each image was georeferenced to a sUAS-derived high resolution orthophotomosaic from 7/11/2017 using 10-50 tie points, depending on availability of consistent reference features (beach park structures and paved pathways change over time). A single analyst carefully digitized the shoreline, using the beach toe as the shoreline proxy. Image contrast and brightness were adjusted to improve delineation of the beach toe as necessary. Shoreline data were processed in the Digital Shoreline Analysis System (DSAS) ArcMap software extension version 4.0, as performed in neighbor island studies (Thieler et al., 2009; Romine and Fletcher, 2013; Anderson et al., 2015).

Table 2. Available historic imagery and associated characteristics for Hāpuna Beach.

Hāpuna Historic Imagery

Date	Scale	Focal Length	Image Area (ha)	Georeferencing Error (m)	Format	Image Source
12/18/1964	1:25,000	unknown	3,000	1.86	B&W	USDA
8/21/1969	1:6,600	151.96	250	0.19	B&W	Unknown (UH Hilo archives)
6/3/1975	1:6,000	151.96	100	1.90	B&W	Hawaiian Aviation
2/4/1977	1:8,000	152.21	350	0.28	B&W	Hawaiian Aviation
12/2/1982	1:25,000	151.96	3,000	0.53	RGB	unknown (UH Hilo archives)
7/17/1987	1:6,000	151.96	100	1.24	B&W	Hawaiian Aviation
5/18/1988	1:6,000	151.96	100	0.57	B&W	Hawaiian Aviation
4/29/2000	1:6,000	151.96	100	2.58	B&W	NOAA

2.2.2.2 Uncertainties

We identified five sources of error similar to Romine et al. (2009) for each individual shoreline vector to reduce any positional and processing bias. Uncertainties for all shorelines are measured at the 95% confidence interval. We determined the total uncertainty of each digitized shoreline to be the root mean sum of squares:

$$E_t = \sqrt{E_p^2 + E_g^2 + E_{toe}^2 + E_s^2 + E_{td}^2} \qquad (1)$$

Pixel error (E_p) is defined as the pixel size of the image (e.g. Romine et al., 2009). Pixel size was as small as 0.02 m for sUAS-acquired orthophotomosaics and 1.49 m for the oldest historic aerial photograph. Previous research has removed imagery with pixel size > 0.5 m, however, removing such images would reduce an already small dataset (Fletcher et al., 2003). Therefore, we do not discard any images due to pixel error.

Georeferencing error (E_g) is defined as the root mean square error produced from georeferencing both historic and sUAS-acquired imagery (e.g. Hapke and Reid, 2007). The georeferencing error is quantified by calculating the difference between estimated and actual positions of tie points and ground control points in the imagery datasets. Our datasets had an E_g range of 0.04 m 2.58 m.

Toe position error (E_{toe}) is quantified to acknowledge any uncertainties in the toe position (i.e. low water mark), which defines the shoreline proxy. We assume that the white wash of the waves masks the true position of the beach toe. Thus, we estimate the beach toe error to be the standard deviation between the landward and seaward positions of the whitewash of the waves.

Seasonal error (E_s) was quantified using shoreline positions from sUAS acquired data and is defined as the variation between mean summer and winter shorelines (e.g. Romine et al., 2009). Summer months were considered as the months from April to September and winter months were considered to be from October through March. We quantified mean summer and winter shorelines by extracting shoreline positions that intersected with transects spaced 20m apart along the beach. The error was determined by computing the standard deviation between the mean summer and winter shoreline positions. Seasonal error was determined to be 7.33 m, and was applied to all shorelines.

Tidal Error (E_{td}) is defined as the standard deviation of shoreline positions measured during a low tide and moderate/high tide. These positions were measured by extracting the low and moderate tide shorelines that intersected with transects spaced 20m apart along the beach and measuring their positional differences.

2.2.2.3. Data Analysis

All shoreline vectors were merged into a single GIS layer that included the shoreline geometry as well as the total uncertainty calculated for each shoreline (Thieler et al., 2009). These data were brought into the DSAS software extension and overlaid with 39 perpendicular transects cast from a defined baseline and spaced approximately 20 m apart (Figure 5). The baseline is the reference point to which shoreline change is measured to, and we delineate it as the 2017 vegetation line. The intersection of each shoreline at each transect was determined and applied to a linear regression using weighted least squares (WLS), which uses the shoreline uncertainties as a weight (Romine et al., 2009; Anderson et al., 2015). This statistical approach reduces the influence of shorelines with higher uncertainties. We followed Romine et al. (2009) to determine the long-term shoreline change rate as the mean of shoreline change rates computed for each transect and reported the uncertainty as the root mean sum of squares of the standard error computed for each transect. We conducted three regression analyses to compare historic shorelines to contemporary shorelines for summer months exclusively (April-September), winter months exclusively (October-March), and all shoreline data sets. We chose this approach in an effort to identify any season-specific changes that might influence the results when analyzing the full dataset.

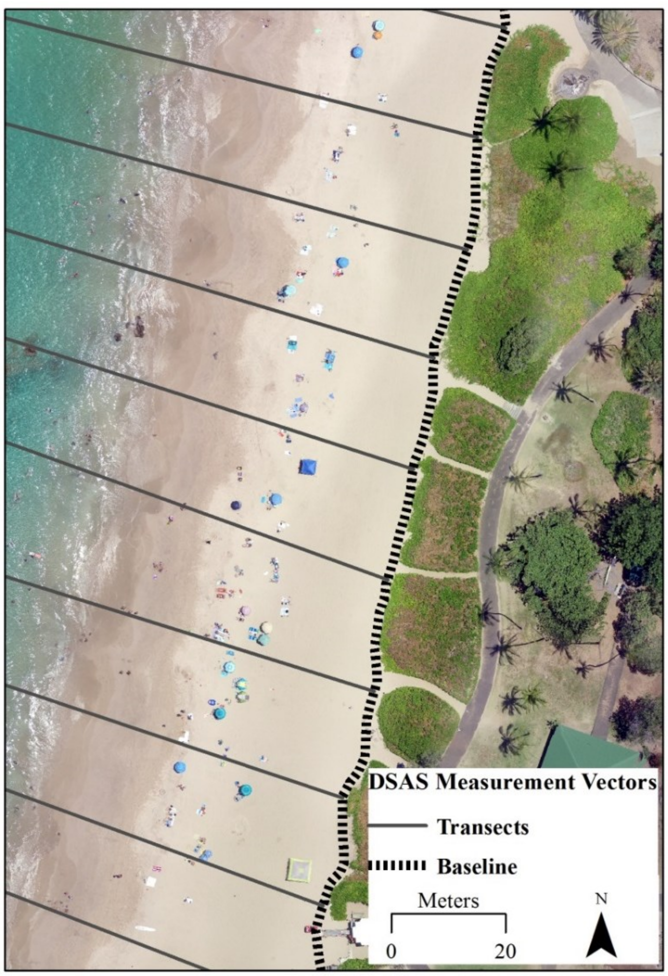

Figure 5. DSAS transect and baseline set up

2.2.3. Hydrostatic Sea Level Rise Modeling

To consider impacts due to climate change, we applied a hydrostatic SLR model (i.e. bathtub model) to each DEM (Marrack, 2015). The hydrostatic modeling approach allows us to conservatively visualize possible impacts under different SLR scenarios and seasonal beach morphology conditions (Marrack, 2015). We use the present epoch mean higher high water (MHHW) as our shoreline reference, which was taken from the NOAA Tides and Currents datum for the Kawaihae, HI tide gauge (#1617433). Then, we added 0.30 m (~ 1 ft) and 0.90 m (~ 3 ft) to the MHHW elevation to visualize SLR expected in Hawai‘i by 2100 (Table 3) (Parris et al., 2012; Sweet et al., 2017; Hawai‘i Climate Change Mitigation and Adaptation Commission, 2017).

Table 3. Calculations used for SLR mapping

Water Level	*SLR Equation*	*Year Expected*
MHHW	1.515m	~
1 ft SLR	1.515m + 0.3m = 1.815m	2039
3 ft SLR	1.515m + 0.9m = 2.415m	2100

2.3 Results

2.3.1. Uncertainties

As described above, we identified five sources of uncertainties for each digitized shoreline. These uncertainties were applied to the shoreline change rate analyses for Hāpuna Beach and had a range of 8.29 m – 23.34 m (Table 4).

Table 4. Uncertainty values computed for each shoreline digitized for Hāpuna Beach.

			Uncertainty Sources			
Year	*Pixel Error (m)*	*Georeferencing Error (m)*	*Tidal Error (m)*	*Seasonal Error (m)*	*Toe Error (m)*	*Total Uncertainty (m)*
12/18/1964	1.49	1.86	3.42	7.33	6.65	10.74
8/21/1969	0.15	0.19	3.42	7.33	6.33	10.27
6/3/1975	0.34	1.90	3.42	7.33	5.10	9.76
2/4/1977	0.21	0.28	3.42	7.33	21.89	23.34
12/2/1982	0.74	0.53	3.42	7.33	7.68	11.19
7/17/1987	0.14	1.24	3.42	7.33	4.20	9.20
5/18/1988	0.15	0.57	3.42	7.33	4.54	9.29
4/29/2000	1.40	2.58	3.42	7.33	2.10	8.86
1/4/2017	0.02	0.05	3.42	7.33	4.55	9.28
3/1/2017	0.02	0.05	3.42	7.33	6.68	10.49
5/1/2017	0.02	0.04	3.42	7.33	5.47	9.76
7/11/2017	0.02	0.03	3.42	7.33	2.08	8.35
9/18/2017	0.02	0.03	3.42	7.33	1.82	8.29
12/5/2017	0.02	0.04	3.42	7.33	3.55	8.83
1/22/2018	0.02	0.03	3.42	7.33	4.09	9.06

2.3.2. Long-term shoreline change

We observe that the shoreline is variable throughout our datasets, but do find that there is a long-term trend of coastal erosion at Hāpuna Beach between 1964 and 2018 (Figure 6). Using WLS, we estimate that Hāpuna Beach has retreated landward at an average rate of -0.18 m yr^{-1} ± 0.17 m since 1969. When observing winter specific shoreline change, we quantify an erosion rate of -0.13 m yr^{-1} ± 0.19 m since 1964. Similarly, when we observe summer-specific shoreline change, we quantify an erosion rate of -0.17 m yr^{-1} ± 0.15 m since 1969.

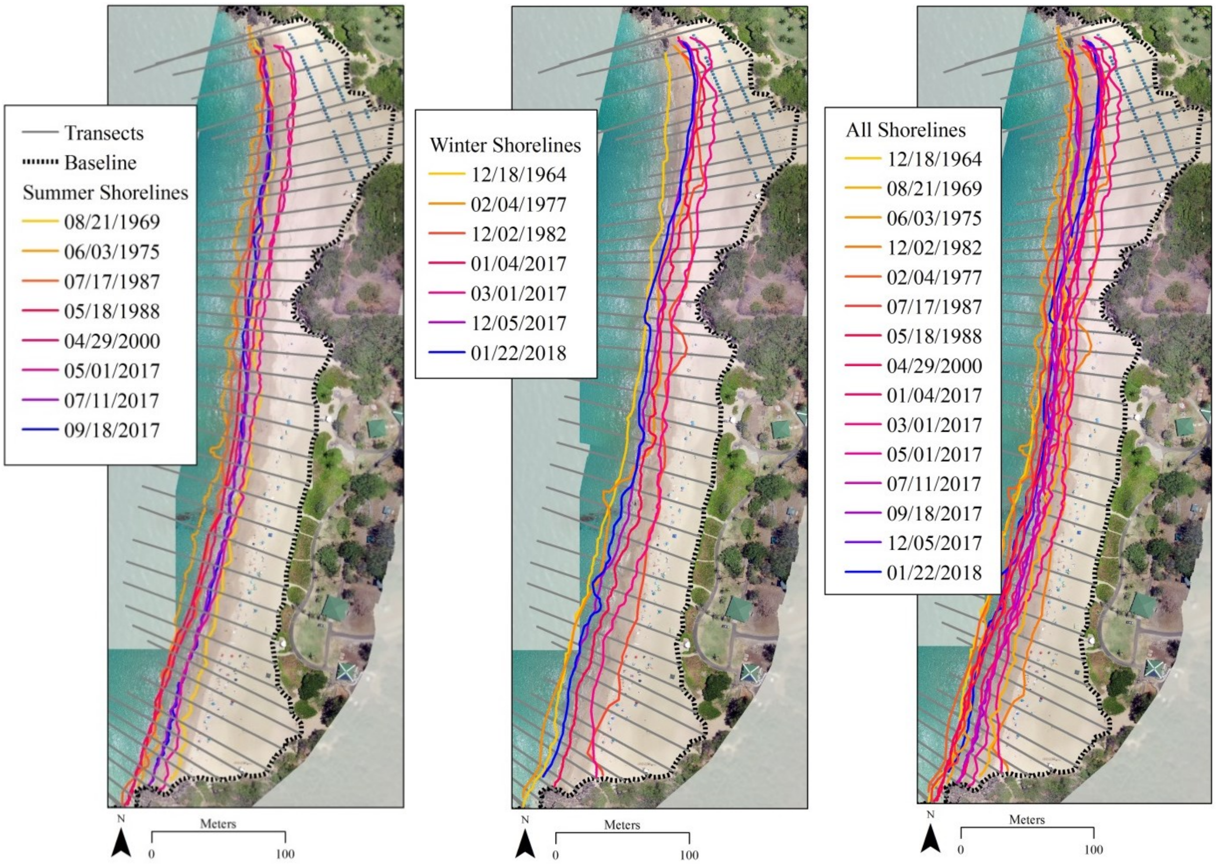

Figure 6. (Left) Summer shoreline Positions, (Middle) winter shoreline positions, and (Right) all shoreline positions.

2.3.3. Short-term shoreline change

Using sUAS, we were able to observe short-term, seasonal change at Hāpuna Beach. We observe patterns of erosion during winter months and accretion during summer months. We used each DEM to map beach erosion and accrual throughout the year (Figure 7). As the beach transitioned into the summer months, we initially observed accretion along the backshore with gradual sand accumulation along the foreshore through July 2017. In September 2017, we observe an episode of erosion concentrated along the north end of the beach. Erosion continued into December 2017 towards the southern end of the beach. There was erosion along the foreshore through the last survey, with some accretion occurring at the interface of the foreshore and backshore. We validated these findings with imagery that show the burial and exposure of a rock outcrop on the beach (Figure 8).

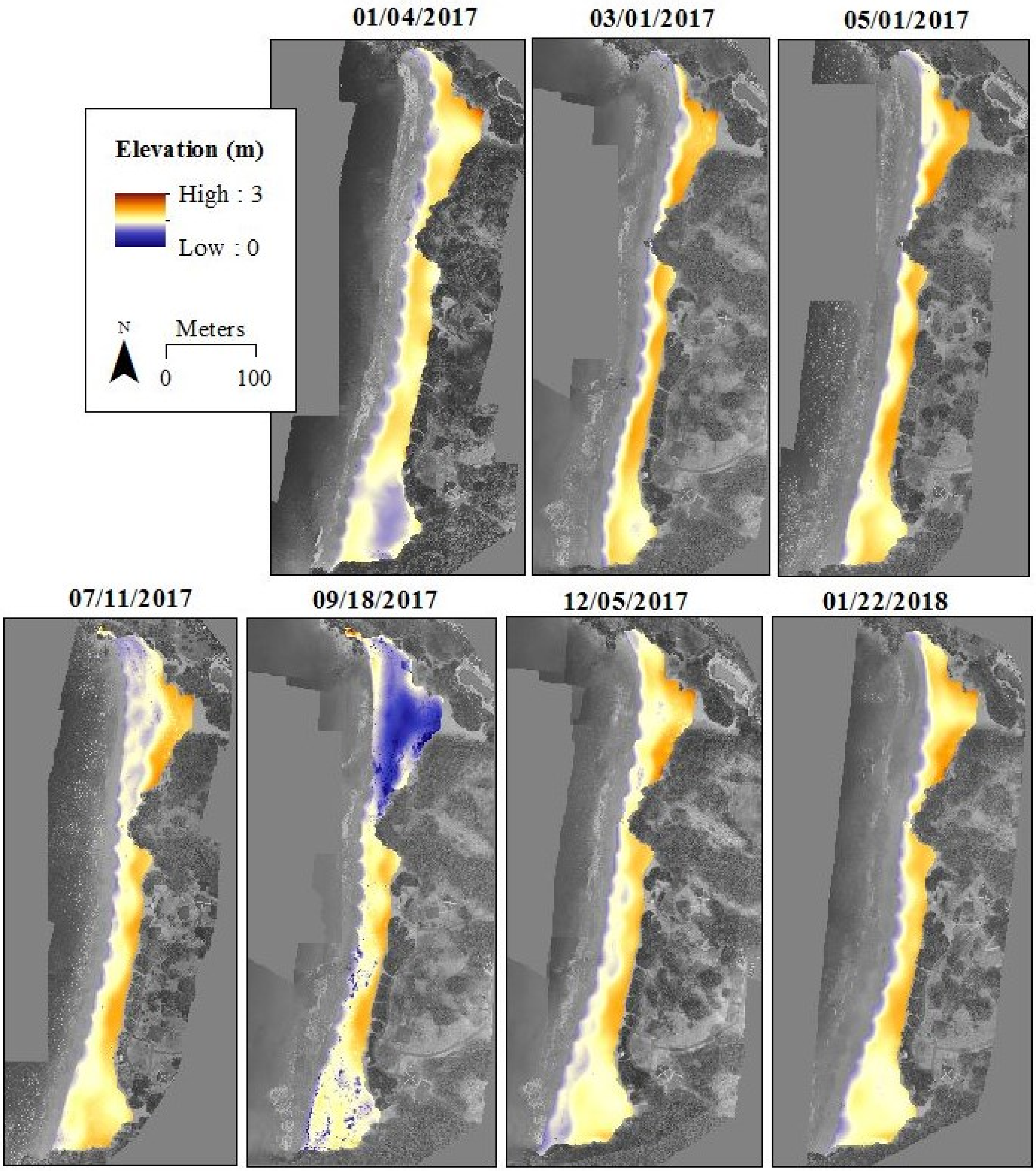

Figure 7. Bare-earth DEM maps for all sUAS dates surveyed.

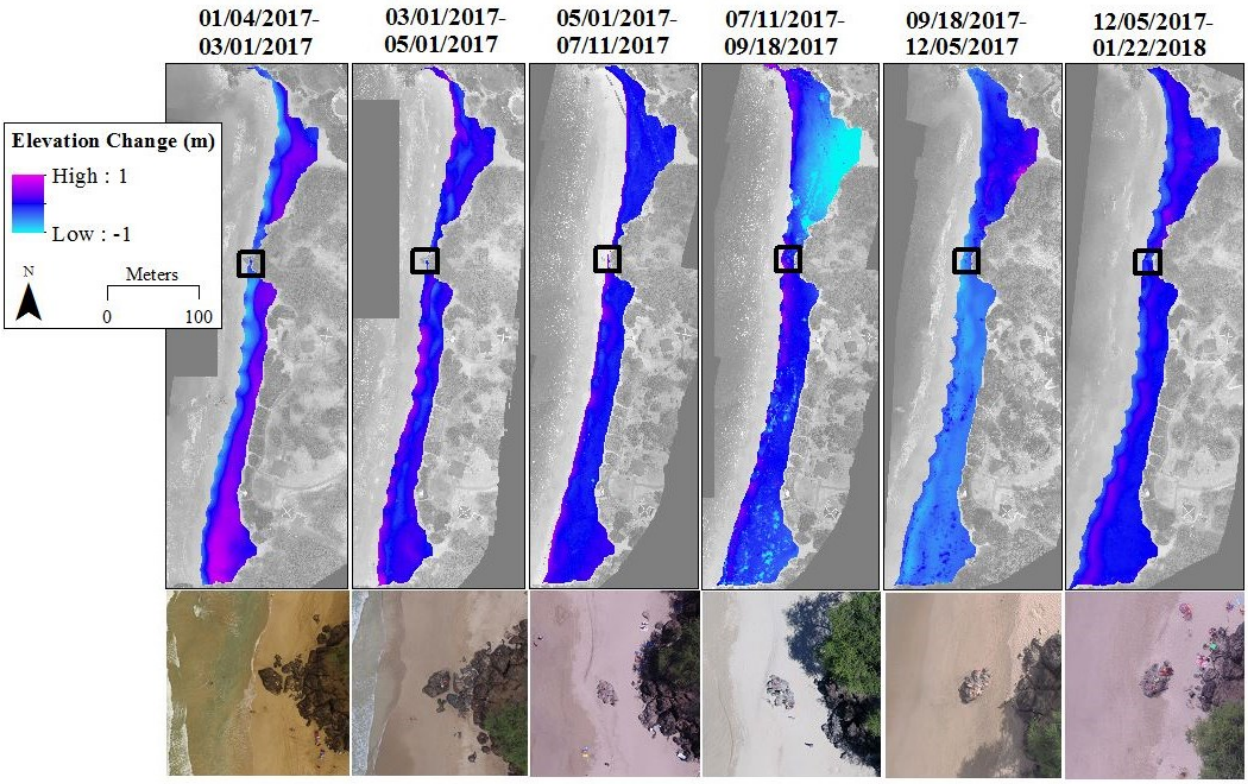

Figure 8. DEM maps highlighting beach sand erosion (bright blue) and accrual (bright pink). Below are images validating intra-annual changes via a rock outcrop by highlighting beach sand erosion and accretion.

We further observe beach area reduction between 0.02 ha (200 m^2) and 0.80 ha (8,000 m^2) during winter months and increases between 0.06 ha (600 m^2) and 0.66 (6,600 m^2) during summer months (Table 4). We observe the greatest mean elevation gain of 1.85 m between January and March of 2017 and the greatest mean elevation decrease of -1.68 m between September and December of 2017 (Table 5).

Table 5. Short-term shoreline change measurements at Hāpuna Beach, HI

Date	*Area (ha)*	*Maximum Elevation (m)*	*Minimum Elevation (m)*	*Mean Elevation (m)*	*Δ Mean Elevation (m)*	*Δ Area (ha)*
1/4/2017	2.39	2.78	0.62	1.52	~	~
3/1/2017	1.59	2.61	0.69	3.37	1.85	-0.80
5/1/2017	1.81	2.53	0.53	1.69	-1.68	0.22
7/11/2017	2.47	2.57	-0.06	1.58	-0.11	0.66
9/18/2017	2.53	3.29	-0.82	1.30	-0.28	0.06
12/5/2017	2.51	2.61	0.74	1.58	0.28	-0.02
1/22/2018	2.23	2.62	0.67	1.63	0.05	-0.28

Shoreline positions were also observed to fluctuate seasonally but do not migrate uniformly throughout the year (Figure 9). Rather, shorelines overlap with each other and vary independent of what season they were observed. We see a mean shoreline positional variation of 7.33 m ± 2.29 m, with the greatest variation in shoreline position occurring at the northern region of the beach.

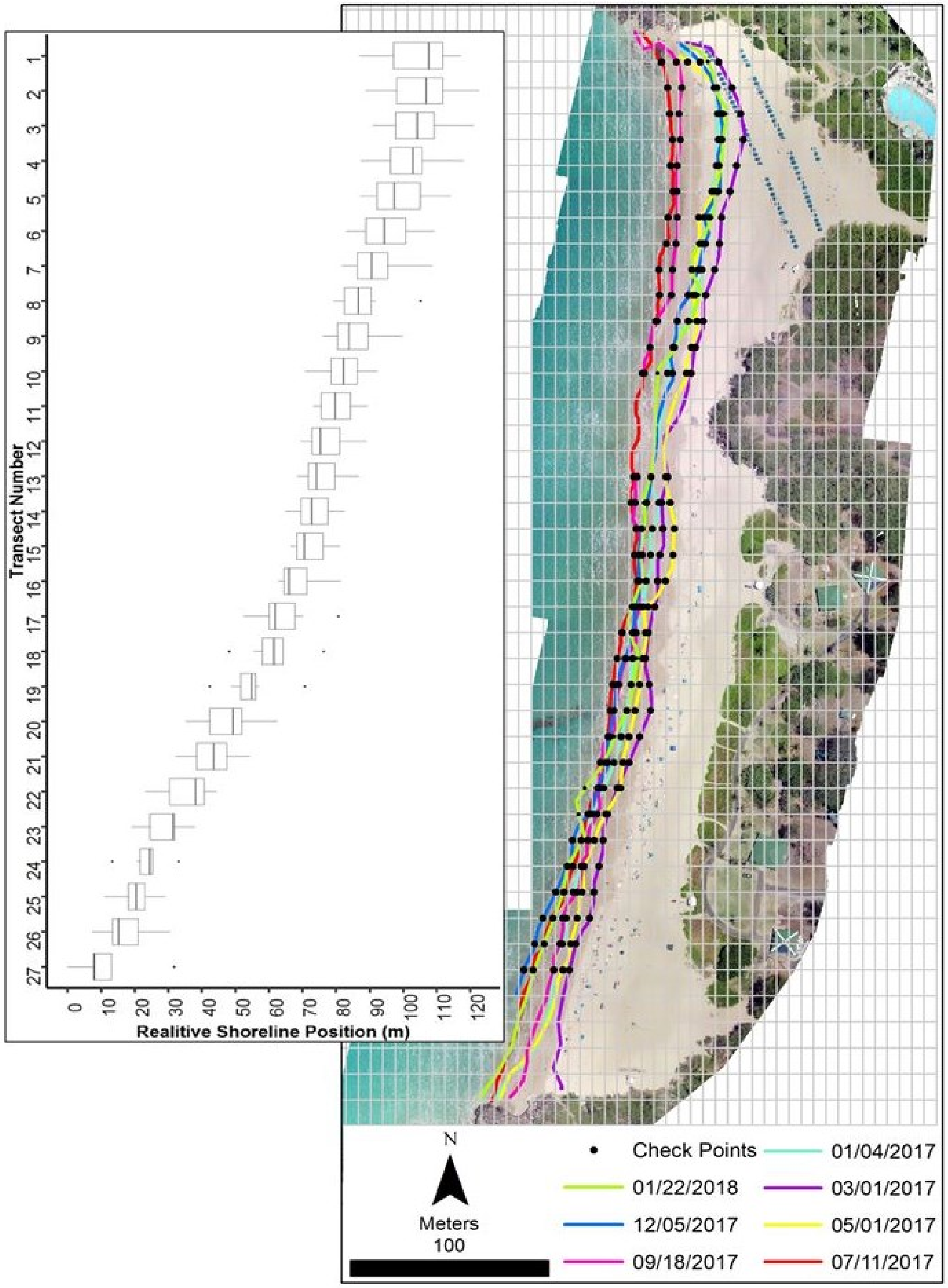

Figure 9. Intra-annual shoreline position variation

2.3.4. Hydrostatic Sea Level Rise Modeling

Using a simple hydrostatic model, we found that 1 ft (0.3 m) of SLR would result in 44% - 49% beach area remaining under worst winter and best summer beach conditions, respectively. In contrast, 3ft SLR would completely submerge the present-day beach regardless of seasonal beach morphology, leaving as little as 6% of the beach remaining. We visualize SLR on the smallest and second largest beach (March and July, respectively) to show potential SLR impacts to distinct seasonal morphologies (Figure 10). We chose the second largest beach because we had more data coverage as compared to the largest beach.

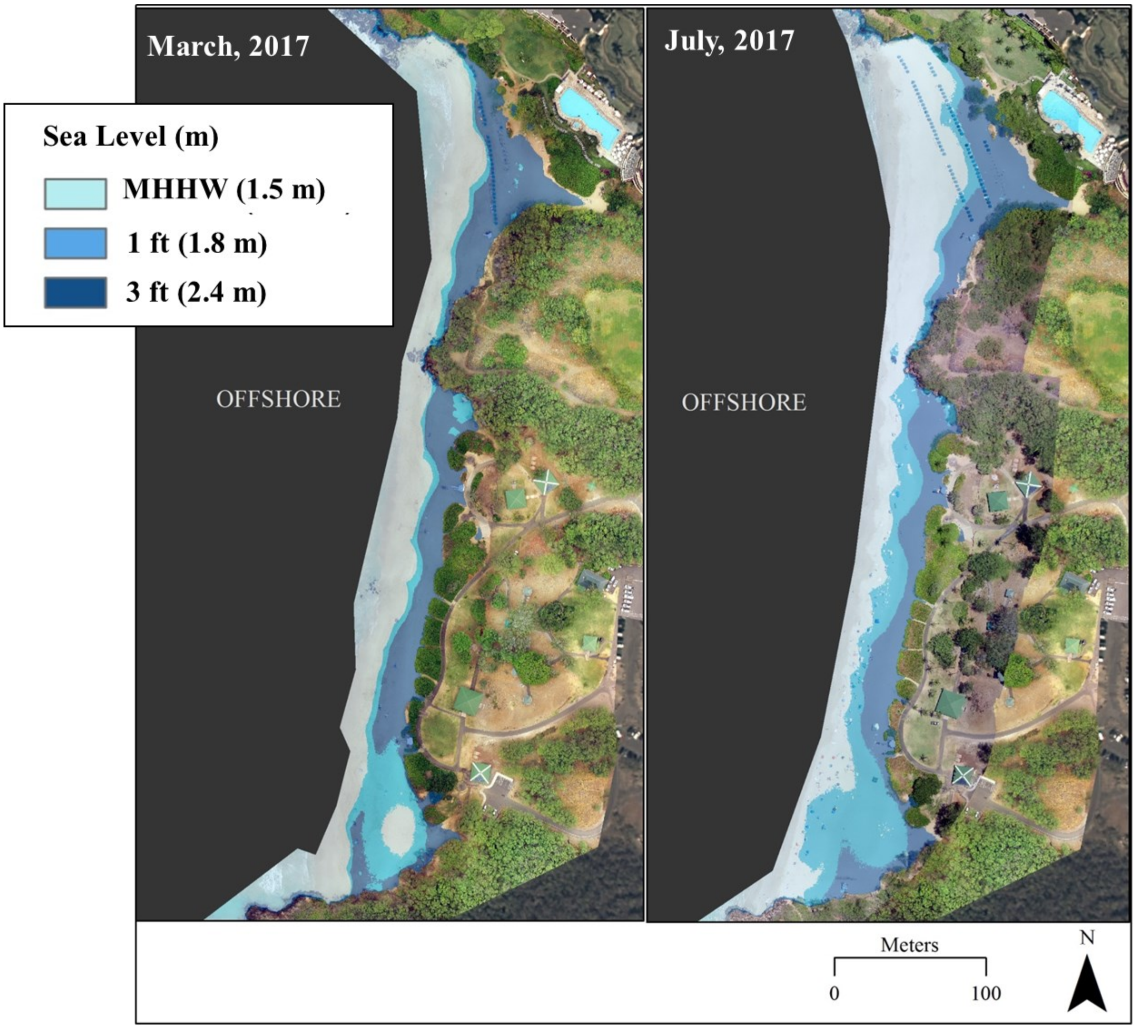

Figure 10. Potential SLR impacts at Hāpuna Beach under 2017 winter and summer beach morphology conditions.

2.4 Discussion

The combination of historic aerial imagery and sUAS datasets are informative for long and short-term shoreline change research. Existing methodologies used on neighbor islands can be used to better understand long-term decadal changes at Hāpuna, and therefore other beaches around the island. Our results reveal that Hāpuna is experiencing overall erosion, although our uncertainty levels are nearly the same as the erosion rates themselves. We report that long-term change is small, while short-term change is large. This could be due to the fact that Hāpuna is a reflective beach and thus may be dominated by long-term erosion and accretion oscillation cycles that are difficult to explain in simplified change rates (van Rijin et al., 2003). As such, Hāpuna Beach may currently be of less concern for significant and chronic beach loss than other neighbor islands are. For example, erosion rates for neighbor islands range between -0.04 m to -0.25 m yr^{-1} with uncertainties that range from ± 0.01m to ± 0.02 m (Romine and Fletcher, 2013). Additionally, a 1991 report described Hāpuna Beach to be eroding at a rate of 0.24 ± 1.52 m yr^{-1} between 1950 and 1988, also suggesting relatively high uncertainty in whether the beach is undergoing significant long-term erosion (Makai Ocean Engineering Inc. and Sea Engineering Inc., 1991). We observe larger variability and uncertainty in the shoreline positions we measured, likely due to the seasonality of the beach. Therefore, long-term beach dynamics here might be more vulnerable to exacerbated seasonality driven by Pacific Decadal Oscillations and El Nino Southern Oscillation-related storm variability.

The addition of sUAS surveys allowed us to gather high resolution information about intra annual beach variability with great accuracy and precision. This is an emerging application of sUAS that has not been widely used, yet greatly advances our understanding of beach dynamics. We can clearly observe seasonal differences in beach size and elevation throughout one year of surveying, with a notable episode of erosion in between July 2017 and September 2017, particularly near the north end of the beach. The loss of sand in September could be due to several factors; there was a powerful two day wind event from September 17- 18, 2017, with maximum gusts of 47 knots (47 miles per hour) (http://windalert.com/wind/spot/1518) that may have redistributed the sand; there was peak steam flow of 16 ft^3 s^{-1} in the Kamuela stream gauges on September 10th which may be indicative of stream flow at the perennial stream at the north end of the beach; the central rock outcropping could have been acting like a break wall built along the shoreline. However, there was no large swell event during the time period that would create the pattern we observe. The other observed seasonal beach loss is likely attributed to strong winter backwash along the beach face, or from rip currents that form along beach cusps during winter months (Aagaard et al., 2013). In contrast, we see beach gain during the transition into summer months. Gentle wave conditions allow sand to be redistributed from offshore and naturally replenish the beach. Thus, our observations are consistent with previous studies that observe beach loss during winter wave conditions and beach gain during gentle summer wave conditions (e.g. Aagaard et al., 2013). These insights on short temporal scales can provide an improved basis for planning and could fill a major knowledge gap validating long- and short-term erosion and accretion oscillations with continued research.

In addition to the long-term and short-term shoreline changes, we reported a conservative estimate of future impacts to Hāpuna Beach as a result of published sea level rise scenarios. We were able to apply bath tub SLR models to DEMs we produced for two distinct seasonal morphologies. While these sea level rise scenarios are not dynamic, they do offer a simple and informative visual for estimating the fate of Hāpuna Beach in the years to come. Our hydrostatic SLR estimates suggest that 1ft of SLR would leave 49% of the beach remaining under best case scenarios, assuming seasonal variability of the beach remained constant. However, more extreme SLR would almost completely eliminate the beach. Fortunately, beaches can migrate landward and adapt to changes as long as they are not constrained by development or topography (Dugan et al., 2010). Hāpuna Beach has no coastal engineering in place to mitigate landward retreat, but beach encroachment may inhibit use of the paved backshore footpath, three rinsing stations, and some grassy landscaping within the beach park and Hāpuna Beach Prince Hotel property. More robust predictive modeling is necessary to understand the full extent to which Hāpuna Beach could migrate under SLR conditions.

2.5 Conclusion

Hāpuna Beach is a highly dynamic beach with several potential forces influencing its morphology, including wave dynamics, wind, and infrequent but significant stream flow. We are able to quantify mean long-term shoreline change rates across various scales, though with variable accuracy despite carefully identifying uncertainties and errors. We do not expect that Hāpuna Beach is under significant threat of erosion, but continued beach monitoring can better inform dynamic processes occurring at this site. A larger dataset and more robust differential GPS surveys in a future study might yield improved results with reduced uncertainties. Further, we were able to quantify complex intra-annual shoreline change with very high accuracy. Thus, we confidently recommend the use of sUAS for further beach monitoring research. Lastly, beaches often get overlooked as a distinct ecosystem, but we can build beach resilience in face of sea level rise by allowing them to naturally migrate without interference of coastal engineering restrictions.

CHAPTER 3: HONOLIʻI BEACH PARK

3.1 Introduction

Sea cliffs are diverse geomorphic features that comprise approximately 80% of the world's coastlines (Emery and Kuhn, 1982). While there is no specific language describing definitive characteristics of these features, sea cliffs generally range in height from a few meters to several hundreds of meters and have slopes that range from 20̊ to 90̊ (Hapke and Reid, 2007). These coastal features are subject to anthropogenic development and various hazards that result in chronic and/or episodic landward retreat (Hapke and Reid, 2007; Dickson et al., 2007; Young, 2018). There is growing concern that sea cliff vulnerability will increase due to rising seas, intensified storms, and increased development demands (Barnard et al., 2016; Hurst et al., 2016). Many developments built along sea cliffs are vulnerable to severe damage induced by erosive forces. In fact, there have been many accounts of properties, roads, and even lives that have been lost due to sea cliff erosion (Young, 2018; Leshchinsky et al., 2017). Extensive research has taken place to better protect and manage development along United States sea cliffs (Barnard et al., 2016; Quan et al., 2013), however, information regarding vulnerabilities and suggestions for sustainable bluff development in Hawaiʻi is sparse.

Currently, Maui is the only county in Hawaiʻi that has implemented a lot-depth setback for properties that are built atop sea cliffs. Maui's setback rule defines the setback to be 25% of a lot's depth and as great as 150 ft for properties with ambiguous shorelines due to cliffs, bluffs, or other topographic features (Maui Planning Commission, 2007). While this policy is a progressive step towards sustainable coastal development, scientific data specific to Hawaiian basalt sea cliffs is lacking. It is therefore critical to understand cliff retreat rates to better inform and encourage coastal cliff-related setbacks statewide, and worldwide. In particular, it is necessary to determine a methodology for identifying the shoreline along sea cliffs as well as quantify long- and short-term changes to the shoreline to produce relevant, place-based setbacks. In this chapter, we use Honoliʻi, a small sea cliff community located on Hawaiʻi Island, as a case study.

Honoliʻi Beach Park (~5 ha) is located on the east coast of Hawaiʻi Island and is characteristic of basalt sea cliffs with pebble beaches at the base of the cliffs (Fletcher et al., 2002) (Figure 11). A statewide assessment of coastal hazard vulnerability ranked the steep cliffs adjacent to Honoli'i Cove as highly vulnerable to erosion, tsunamis, high waves, and storms (Fletcher et al., 2002). Development of this region began in the 1950s, prior to any hazard assessment, and it is now a residential community and popular beach park. Six properties have been built directly on the edge of the cliff, with one property, defining our specific study site, visibly subject to severe cliff erosion and subsequent property damage (Figure 11). This particular property has been remodeled several times in response to the cliff failure, however, foundation and terrigenous debris continue to fall near the beach park and into the surf zone. The persisting environmental and human safety hazard has led the County of Hawaiʻi to require the property be remodeled again by September 2018. Thus, this research informs the County of Hawaiʻi, homeowners, and recreational users of cliff retreat hazards here, and what might be expected for other developed sea cliffs along Hawaiʻi's coast.

This chapter will discuss our scientific process for understanding cliff retreat at Honoliʻi and implications for sustainable coastal cliff management. It is important to note, however, that we do not attempt to apply any hydrostatic SLR modeling like the other chapters in this manuscript due to the sea cliff not being vulnerable to sea level rise. Instead, we focus on past and present cliff retreat and potential increased vulnerabilities due to a changing climate.

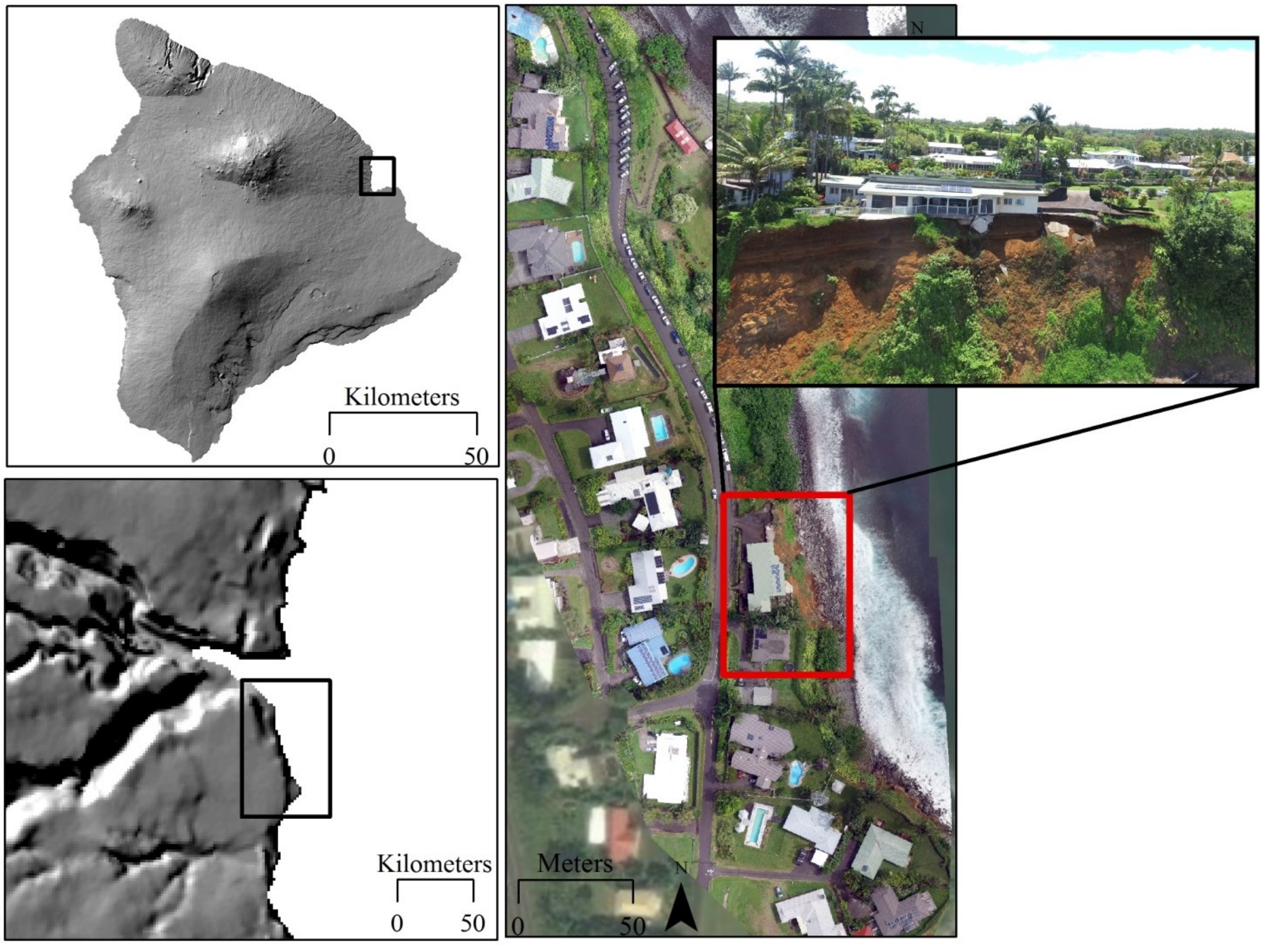

Figure 11. Map of the Honoli'i sea cliff study site; hillshade data for left two panels is from the state of Hawai'i GIS database.

3.2. Methods

3.2.1 Short-term cliff edge change

We use similar methods described in 1.2.1 for collecting sUAS imagery at Honoli'i. The DJI Inspire 1 sUAS platform was used with the DJI Zenmuse X3 camera to capture change over time. Imagery was acquired at Honoli'i every month from January 2017 until January 2018, with the exceptions of May 2017, July 2017, and November 2017 due to data backup failure and restricting weather conditions (Table 5).

Table 6. sUAS imagery collected and processed for cliff top change analysis

Date	*Pictures Taken*	*Pixel Size (m)*	*RMSE (m)*
1/13/2017	281	0.02	0.03
2/15/2017	264	0.02	0.03
3/2/2017	251	0.02	0.02
3/17/2017	297	0.02	0.02
3/20/2017	303	0.02	0.02
4/28/2017	235	0.02	0.02
6/28/2017	149	0.02	0.01
8/13/2017	129	0.02	0.03
9/26/2017	398	0.02	0.01
10/17/2017	299	0.02	0.01
12/8/2017	222	0.02	0.04
12/27/2017	204	0.02	0.02
1/24/2018	281	0.02	0.03

sUAS flights were conducted at 45 m altitude during low tide and parallel to the shoreline/top of the sea cliff to render orthophotomosaics of the site at ~ 0.02 m resolution (Goncalves and Henriques, 2015; Yoo and Oh, 2016; Casella et al., 2016). Elevation change analysis was done over using the digital surface models (DSMs) produced in Pix4D with no additional processing, to avoid potential errors introduced in this sheer cliff environment through attempts to remove vegetation and buildings. DSMs for all dates surveyed were produced at 0.02 m resolution and accurate to ± 0.07 m. We determined the DSM accuracy by comparing the position of 99 consistent independent check points across all DSMs, and report the mean standard deviation of those points at the 95% confidence interval.

Cliff top retreat and erosion was measured similar to section 2.2.1 and 2.2.2; we digitized shoreline vectors for each dataset to measure shoreline position retreat throughout the year. We referred to 3 dimensional point cloud data to ensure undercut regions of the property in place did not falsely represent the cliff edge (Figure 12). All data were projected in WGS 83 for UTM Zone 5.

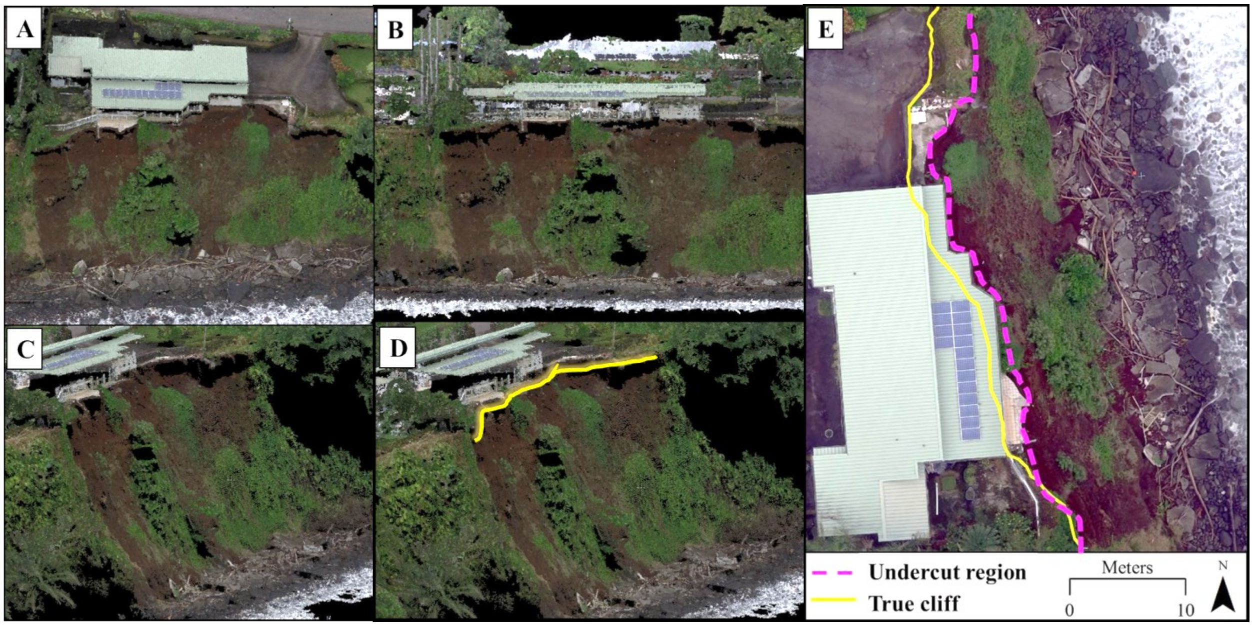

Figure 12. (A-C) Three dimensional point cloud perspective used to differentiate between the cliff edge and undercut regions; and (D-E) delineation of the cliff edge shoreline (yellow solid line) versus undercut regions (pink dashed line).

3.2.2. Long-term cliff edge change

We quantify long-term shoreline change by applying the same methods described in 2.2.2. We gathered all available historic aerial photographs from Hawai'i County, the UH Hilo Hilo Geography Department, and MAGIS program. We selected nadir images that had a scale ≥ 1:50,000 and were in sharp focus. Based on these criteria, we gathered a total of 4 images that were scanned at a resolution between 720 and 1200 dpi (Table 7). Each image was georeferenced to a high resolution orthophotomosaic using 20-50 tie points, depending on availability of consistent reference features. A single analyst carefully digitized the shoreline using the top edge of the sea cliff as the shoreline proxy (e.g. Hapke and Reid, 2007). This shoreline proxy is defined as the distinct change in slope from the top of the cliff to the face of the cliff. In the historic aerial photographs, this is distinguished by altering the contrast and brightness of the image, where the top of the cliff is typically lighter and the transition to cliff face is obviously darker due to shadows.

Table 7. List of imagery used for Honoli‘i, HI, and associated characteristics

Date	*Scale*	*Focal Length*	*Image Area (ha)*	*Georeferencing Error (m)*	*Format*	*Provider*
9/15/1964	1:20,000	151.96	3,000	1.12	B&W	USDA
1/16/1965	1:20,000	unknown	3,000	1.32	B&W	USDA
1/22/1976	1:6,000	152.21	150	1.87	B&W	Hawaiian Aviation
7/25/1987	1:6,000	151.96	150	0.03	B&W	Hawaiian Aviation

Further following Hapke and Reid (2007), we identified two primary sources of error for each individual shoreline to reduce positional and processing biases. We use the same definitions for the georeferencing error, pixel error, and total uncertainty as section 2.2.3. All shoreline vectors were processed in DSAS using the earlier described methodologies, with the addition of an end point rate analysis (EPR). We use an EPR to determine the difference in clifftop position between the earliest and most recent clifftop edge. We define our baseline to be the road that runs parallel to the shoreline.

3.3 Results

3.3.1 Uncertainties

We were able to quantify uncertainties for each historic shoreline by determining the georeferencing and pixel errors and using those values to determine the total uncertainty. We find an uncertainty range of ± 0.04 m - 2.59 m for the cliff edge shoreline dataset and report these errors at the 95% confidence interval (Table 8).

Table 8. Uncertainty ranges for each cliff edge by date

Uncertainty Source	12/15/1964	1/16/1965	1/22/1976	7/25/1987	01/24/2018
E_g, georeferencing error (m)	1.12	1.32	1.87	2.58	0.03
E_p, pixel error (m)	0.47	0.58	0.20	0.23	0.02
E_t, total positional error (m)	1.21	1.44	1.88	2.59	0.04

3.3.2. Long-term shoreline change

Our historic datasets reveal cliff retreat that has resulted in property damage where there is active erosion. Our DSAS analyses determines that the top edge of the Honoliʻi sea cliff has receded a maximum of 9.5 m in 54 years with an EPR of -0.12 ± 0.01 m yr^{-1} (Figure 13). The WLR is in close agreement with the EPR and indicates that the edge of the Honoliʻi sea cliff has been eroding at a rate of -0.13 ± 0.26 m yr^{-1}.

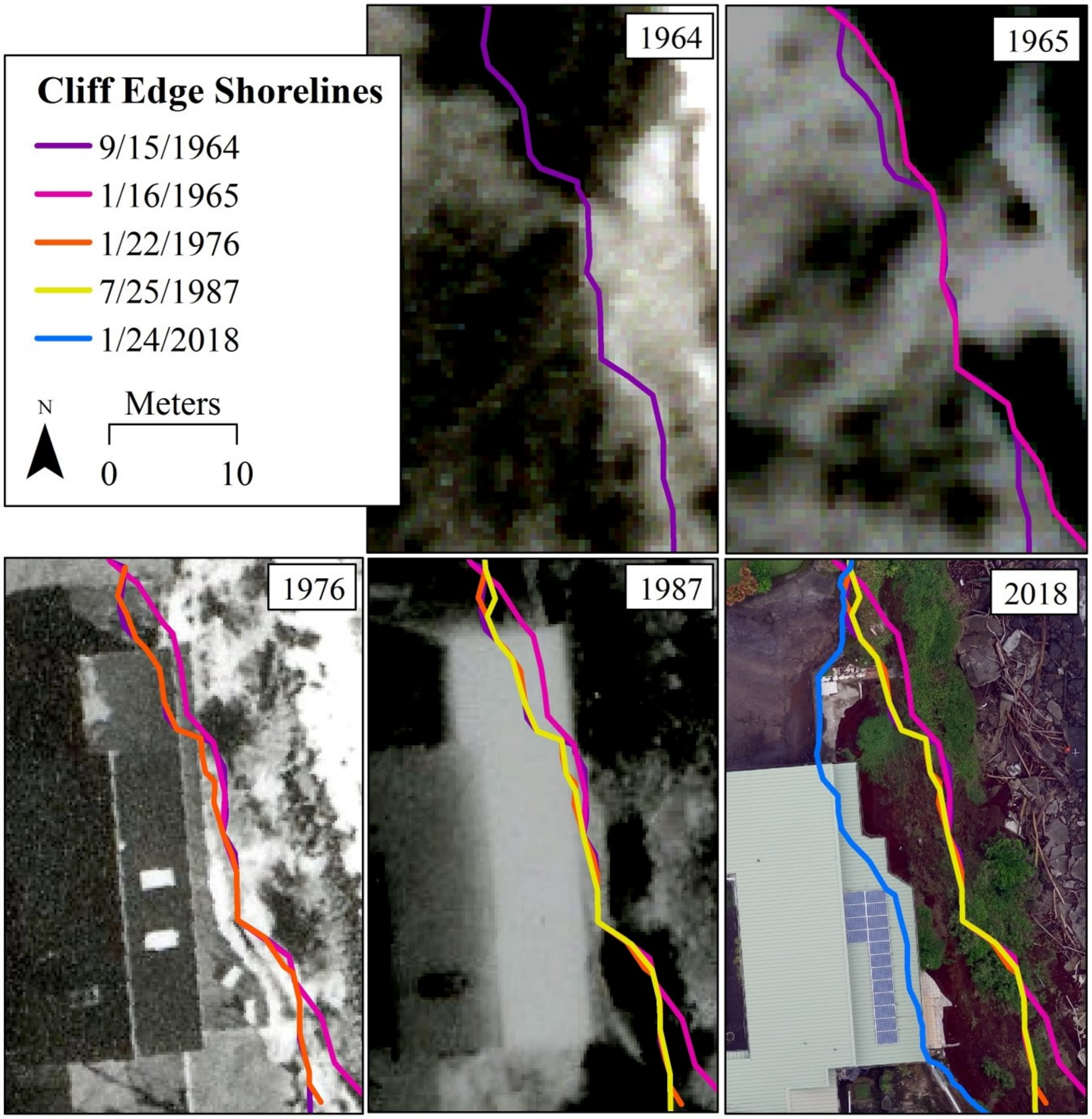

Figure 13. Visible cliff retreat between 1964 and 2018.

3.3.3 Short-term shoreline change

During our one year of data collection, the Honoliʻi sea cliff receded a maximum of 2.44 m ± 0.02 m in one location (Figure 14). A total area of 34.5 m^2 was eroded in this time. Cliff edge retreat is not consistent over time, evident in episodic, short-term events that were recorded using the sUAS data. One event in particular between September 2017 and December 2017 resulted in maximum land retreat of 0.56 m ± 0.02 m. Oblique and ground-based photos also show regions where the cliff is being undercut, and consequently causing further deposition of cement foundation, patio tiling, and sediment to the base of the sea cliff (Figure 15).

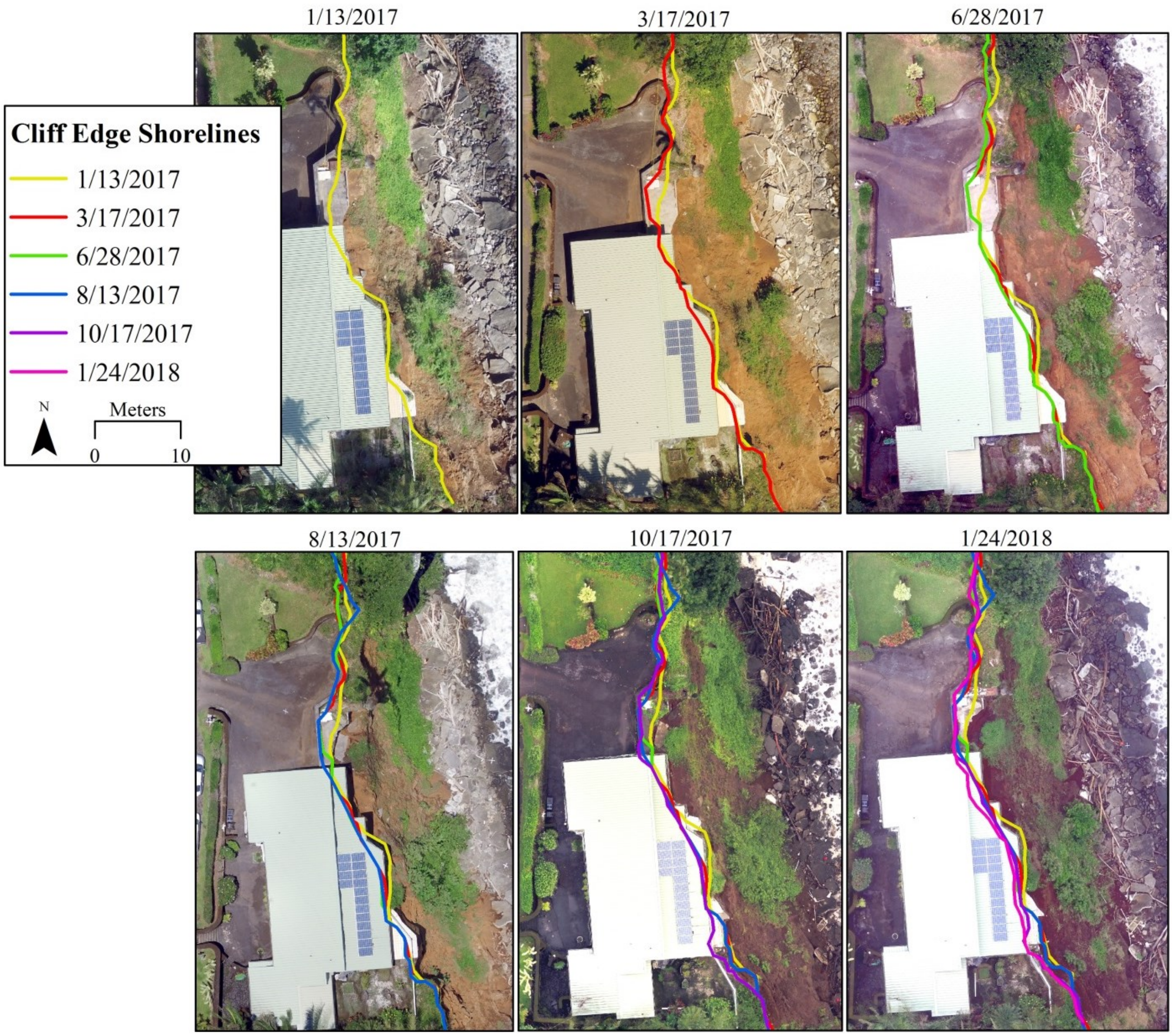

Figure 14. Subset of shoreline positions and associated orthophotomosaics at Honoliʻi between January 2017 and January 2018.

Figure 15. Undercutting of the property and sea cliff, and subsequent debris deposition at the base of the cliff.

3.4. Discussion

3.4.1 Long-term shoreline change

Using historic aerial images, we determined that cliff edge retreat across the study site ranged from of 0 m - 9.5 m between 1964 and 2018 across the study site. We were also able to use those data to determine an end point rate of change of -0.12 m ± 0.01 m $^{yr-1}$, and a similar rate of -0.13 m yr^{-1} ± 0.26 m using weighted linear regression. However, we are skeptical of the error associated with these reported change rates and expect that a follow up analysis comparing DSAS error statistics with the positional differences from our total station surveys will yield a larger uncertainty for these change rates. It is also important to note that we do not identify a cliff edge position error due to a lack of identifiable features that adequately represent other possible shoreline positions. Therefore, the change rates we produce may be overestimated than if further consideration went into identifying other uncertainties. Additionally, we know that cliff top retreat is primarily episodic, as opposed to a steady, linear loss (Hapke and Reid, 2007). Unfortunately, there are very few historic data available to identify specific periods of loss within a decade, let alone within a year, along the Honoliʻi Coast. Thus, it still unknown how many events occurred that contributed to the total retreat observed in the past 54 years. Despite this data gap, we did identify two periods of obvious retreat within the one year of sUAS surveys, and could assume that previous years have experienced similar patterns of loss.

The current property owners have discussed that the cliff face was hardened in 2013 in an attempt to inhibit further erosion, but that coastal engineering effort failed after two heavy rainfall events that occurred between 2013 and 2014. As a result, the cement hardening collapsed, bringing down chunks of the cliff with it. We do not know how much this event contributed to the retreat of the sea cliff thus far and therefore recommend that a future study performs an analysis using available Pictometry datasets to estimate changes along the Honoliʻi sea cliff during the 2000s. Pictometry datasets were not included in the analysis because they were not nadir and therefore required additional processing beyond the scope of this project. In the absence of ample historic datasets, our long-term observations of change can be interpreted as conservative, worst-case scenario, examples of what could continue to happen at Honoliʻi into the future.

3.4.2. Short-term shoreline change

The application of sUAS greatly aids the pursuit of understanding changes occurring along the cliff that historic datasets do not show due to their limited temporal scale. Furthermore, sUAS allow for improved investigation of the entirety of a cliff via structure from motion photogrammetry, in which we are able to recreate the cliff environment in three-dimensional space and in high detail (Dewez et al., 2016). Between January 2017 and January 2018, we determined a maximum cliff retreat of 2.44 ± 0.02 m in one location, and a period of episodic loss between September 2017 and December 2017 that resulted in maximum cliff retreat of 0.56 ± 0.02 m. This is a massive improvement compared to traditional approaches of quantifying cliff retreat using historic aerial imagery, or even lidar, because we are able to monitor changes to the cliff at a much shorter temporal scale and at low cost (Dewez et al., 2016; Barlow et al., 2017). sUAS also enable the ability to adjust the camera angle to get data of the cliff face and regions subject to undercutting that lidar and historic aerial photos do not effectively capture.

Using sUAS, we were able to capture episodes of erosion and periods of little to no cliff retreat. The combination of high resolution imagery and digital surface models allowed us to identify a cliff top shoreline and perform change analyses. Our observations suggest that the cliff does not retreat in a uniform manner, but rather undergoes infrequent but significant periods of loss. Additionally, we can see property damage that coincides with cliff retreat and identify where the property may be most vulnerable due to undercutting of the sea cliff. The observed losses may be attributed to the declining structural integrity of the property itself, or a result of other forces such as wave impact and heavy rainfall events that erode the cliff (Tsunamura, 2015; Johnstone et al., 2016). These data are extremely informative for addressing hazardous and vulnerable coastal developments. The methods we used in this study can be directly applied to establish a relevant cliff edge shoreline boundary and create relevant place-based sea cliff setbacks based on worst case scenario episodic events, rather than arbitrary distances. Thus, sUAS are a useful tool for monitoring shoreline change along sea cliff environments and for informing vulnerabilities to developers, county and state planners, and community residents, who may not know the risks associated with building and living along certain sea cliff environments.

3.4.3. Future Changes

Given that cliff retreat is primarily driven by episodic events, long-term change rates are not necessarily appropriate for estimating future retreat. Many sea cliff communities worldwide experience intensified erosion events during climate oscillations (e.g. El Niño), and research suggests that these events will occur more frequently if the global climate continues to change as expected (Dickson et al., 2007; Quan et al., 2013; Johnstone et al., 2016). These climatic events are associated with strong waves that can cause significant coastal erosion and property destruction, which was famously reported in Pacifica, California, in 2014, by the New York Times and other local news agencies (e.g. “El Nino Storms Put Pacifica Cliff Apartments at Risk,” The New York Times). Monitoring efforts along other sea cliff environments using laser scanning and sediment sampling techniques have also shown relationships to cliff retreat and increased storminess (Lim et al., 2005; Hurst et al., 2016). Honoliʻi, and other sea cliff communities throughout Hawaiʻi and beyond, are likely not an exception to increased sea cliff retreat resulting from increased storm conditions. If severe El Niño conditions become the norm later into the 21st century, present-day episodic sea cliff retreat could be a proxy for future erosion (Quan et al., 2013).

With this information in mind, we recommend Hawaiʻi County planners consider present-day episodic retreat measurements for estimating future retreat along the Honoliʻi sea cliff, and similar environments. For example, planners can assume an episodic event occurs at this site at least once a year with a maximum cliff edge retreat of 0.56 ± 0.02 m yr^{-1}. Based on these data, the maximum cliff edge retreat could be used to establish an aggressive shoreline setback by acknowledging erosion events that are not accurately represented in long-term change rates. However, Hawaiʻi County Planners could also use the erosion rate from the EPR or WLR (~ -0.12 ± 0.01 m yr^{-1}) to establish a less aggressive, yet still scientifically supported shoreline setback. Regardless, continued monitoring using sUAS can better inform the frequency of these erosive events and how they can be scaled up to more accurate predictions of future sea cliff retreat.

3.5 Conclusion

In summary, this study demonstrates the capabilities of sUAS to identify and monitor coastal hazards within a small sea cliff community on Hawaiʻi Island's east coast. We are able to combine historic aerial imagery and sUAS to determine long- and short-term cliff retreat rates for the Honoliʻi sea cliff and observe subsequent development changes that took place in response to the cliff retreat. While historic datasets limit the ability to identify important periods of cliff retreat and sediment deposition, continuous monitoring via sUAS provides key insights to when an episode of erosion approximately occurred and how much the cliff edge retreated. We also report the ability to acquire more information about the cliff face and identify regions where the cliff is undercut and posing an eminent threat to existing development.

CHAPTER 4: KAPOHO (VACATION ESTATES)

4.1. Introduction

Due to past and ongoing volcanic activity, Hawaiʻi Island is impacted by subsidence, particularly on the south east coastline. Subsidence is the downward vertical movement of land due to earth surface deformation from tectonics, volcanism, and glaciation, and greatly influences relative sea level (Galloway et al., 1999; Haer, 2013; Conrad, 2013). Subsidence and its influence on sea level rise has been studied throughout the world. A study conducted by Marther et al. (2009) found that vertical crustal movements increased the trend of sea level rise at Port Nolloth, South Africa, to nearly 1 cm yr^{-1}. While the cause of subsidence in South Africa is from glacial sheet ice loading, results from Marther et al. (2009) provide insight to other geologically active coastal regions, like Hawaiʻi, that may consequently have increased projected sea level rise.

Significant subsidence was measured during major seismic events on the south east coast of Hawaiʻi Island in 1868 and 1975, when the elevation dropped as much as 2 meters and 3.5 meters, respectively (Hwang, 2007). Kapoho, a coastal community (~ 20 ha) on the south east coast of Hawaiʻi Island (Figure 16), experienced abrupt subsidence of 0.25 m following the 1975 earthquake and has since become an area of interest for understanding the natural hazards that threaten community resilience (Hwang, 2007). Part of the Kapoho community is built atop low lying (<1.5 m elevation) lava fields and is estimated to experience annual subsidence of 0.7 - 1.6 cm (Hwang, 2007). This region is also subject to sea level rise rates of 0.8 - 1.7 cm yr^{-1}, and thus may be threatened by the combined effects of sea level rise and subsidence given its already low elevation (Fletcher et al., 2002; Hwang, 2007). Additionally, the Kapoho community sustains a series of inland anchialine ponds, which have no surface connection to the ocean, but are tidally connected by groundwater; as the ocean tide rises, so do the water level in the anchialine ponds. As a result, sea level rise may also cause inland flooding via anchialine pond over flow and even lead to the emergence of new ponds (Marrack, 2016).

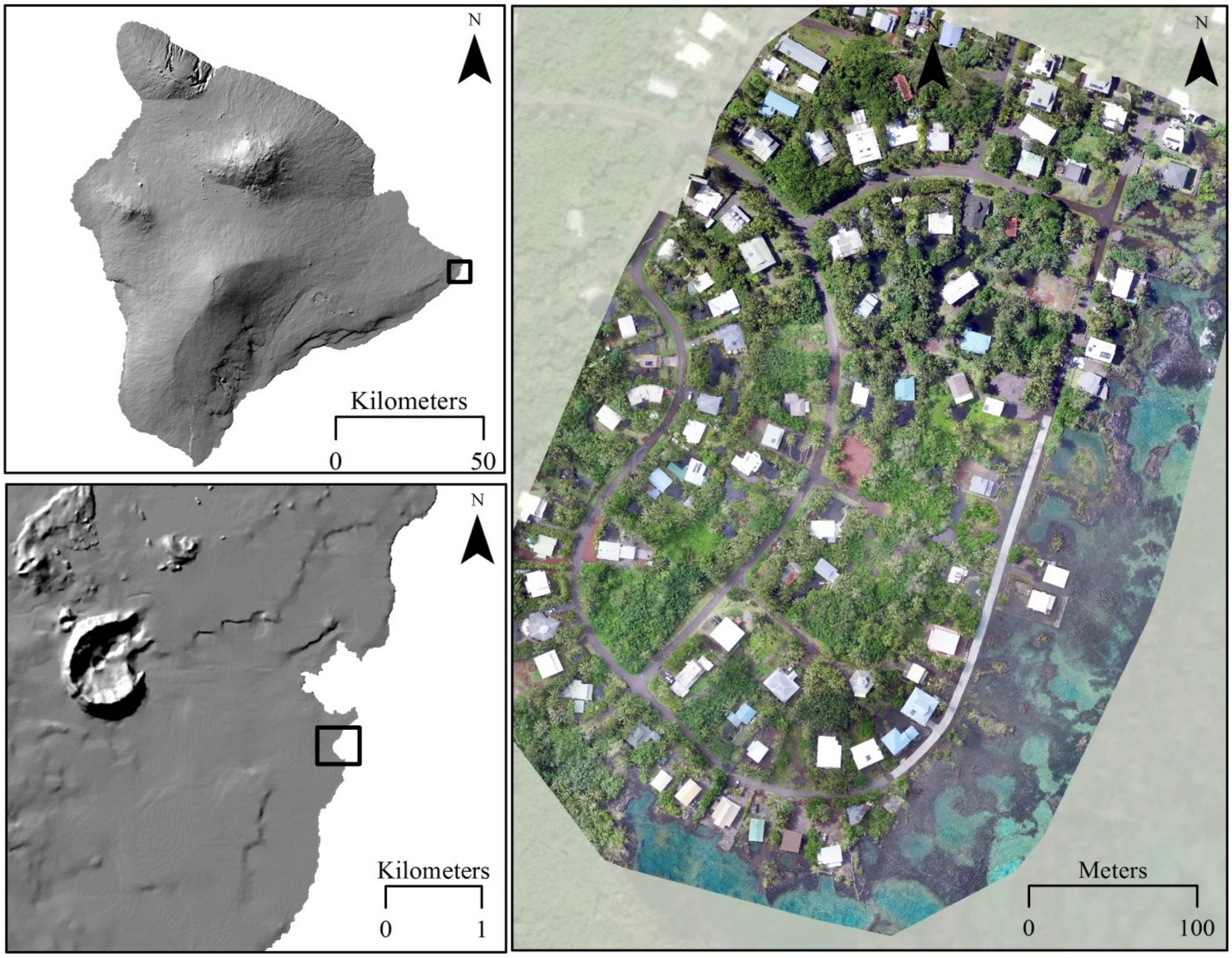

Figure 16. Map of the Kapoho community study site; right panel shows the study area via a high resolution orthophotomosaic derived from a sUAS; hillshade data for left two panels is from the state of Hawaiʻi GIS database.

Residential development began here in the 1950s, with many homes built up to the edge of the water prior to any coastal hazard assessment. Hawaiʻi County's shoreline setback policy has yet to account for processes like subsidence and sea level rise, and thus has not effectively prevented unsustainable coastal development at Kapoho. There are a total of 143 parcels within the study site, many of which regularly experience nuisance flooding during normal high tides, which might be exacerbated due to the ongoing subsidence and causing anchialine pond over flow (Hwang, 2007; Dow et al., 2009; Marrack, 2016). Throughout the years, coastal processes and storm events have caused property and road damage, and even prompted the demolition of at least five homes after Hurricane Iselle passed south of the community. Additionally,all properties in the Kapoho community have on-site waste disposal systems (OSWDS) (i.e. cesspools and septic tanks) that contribute up to 27% of hazardous nitrogen inputs to the Wai‘ōpae tide pools, an adjacent marine protected area (Wiegner et al., 2016). Despite efforts to restore and preserve infrastructure and development of the Kapoho community, hazardous coastal processes persist.

Unlike the Hāpuna and Honoli‘i, erosion is not a major coastal vulnerability for Kapoho because of the basalt shoreline and negligible sediments. Therefore, we focus on identifying nuisance flooding and SLR vulnerabilities to this community. The objective of this study was to estimate the combined impacts of sea level rise and subsidence into the future at this site. We achieved this goal by producing a high-resolution DSM of the Kapoho community using differential GPS equipment and sUAS, applying a hydrostatic model to the DSM, and identifying how many properties and onsite waste disposal systems (i.e. cesspools and septic tanks) might be impacted by inundation. We also conducted a sUAS survey during an extreme high tide (king tide) flooding event to determine present day vulnerabilities to Kapoho.

4.2. Methods

4.2.1. Data Acquisition

We use a combination of sUAS-acquired imagery and differential topographic surveys to identify nuisance flooding hazards, and map expected change based on existing SLR and subsidence data produced by previous work (Hwang et al., 2007; Parris et al., 2012). We conducted two sUAS surveys using similar methods described in sections 1.2.2. and 2.2.2. We established a total of 24 GCPs throughout the study site to georectify the sUAS imagery. We surveyed during low tide on October 23, 2017 to identify anchialine ponds prior to any tide related over flow. We also surveyed during the June 23, 2017 king tide event, which allowed us to collect data of an extreme tide indicative of 1ft of SLR. We use the June 2017 DSM for further SLR analyses. Our sUAS surveys were conducted at 45 m altitude and covered an area of ~ 15 ha. The accuracy of the orthophotomosaics was defined as the RMSE computed in Pix4D software. The error of the DSM was determined by computing the mean difference of GCP elevation values of the DSM and true surveyed elevations of the GCPS. All error estimates are reported at the 95% confidence interval.

4.2.2. Data Analysis

We generated a 0.02 m DSM in Pix4D using the sUAS and ground control data acquired during the June 2017 king tide survey. We used ArcMap 10.5 to digitize the local MHHW (1.927 m) derived from the Hilo tide gauge (#1617760), as well as the 20 ft and 40 ft setback boundaries established by the state and county, on to the DSM. The setback boundaries were identified by creating a 20 ft and 40ft buffer around the designated shoreline, which is loosely described by the County of Hawaiʻi as Waiʻōpae Road (B. Morrison, personal communication, July 22, 2015). We did this to visualize where the established setback boundaries are relative to the present-day average highest reach of the sea water. Additionally, we used the October 2017 orthophotomosaic to digitize all existing anchialine pond boundaries prior to any exacerbated extreme tide flooding (Figure 17). We used the June 23, 2017 king tide orthophotomosaic to manually digitize the reach of the extreme water level and any inland flooding. This was done by carefully tracing the boundary of saturated and dry ground where the ocean directly flowed, and where there was inland anchialine pond flooding (Figure 17). We determined present-day impacts by overlaying a Kapoho tax map key (TMK) and a local OSWD GIS layer with the digitized water level positions and flooded areas. From the TMK we identified how many parcels, either developed or developable, and OSWDS were exposed to any amount of flooding.

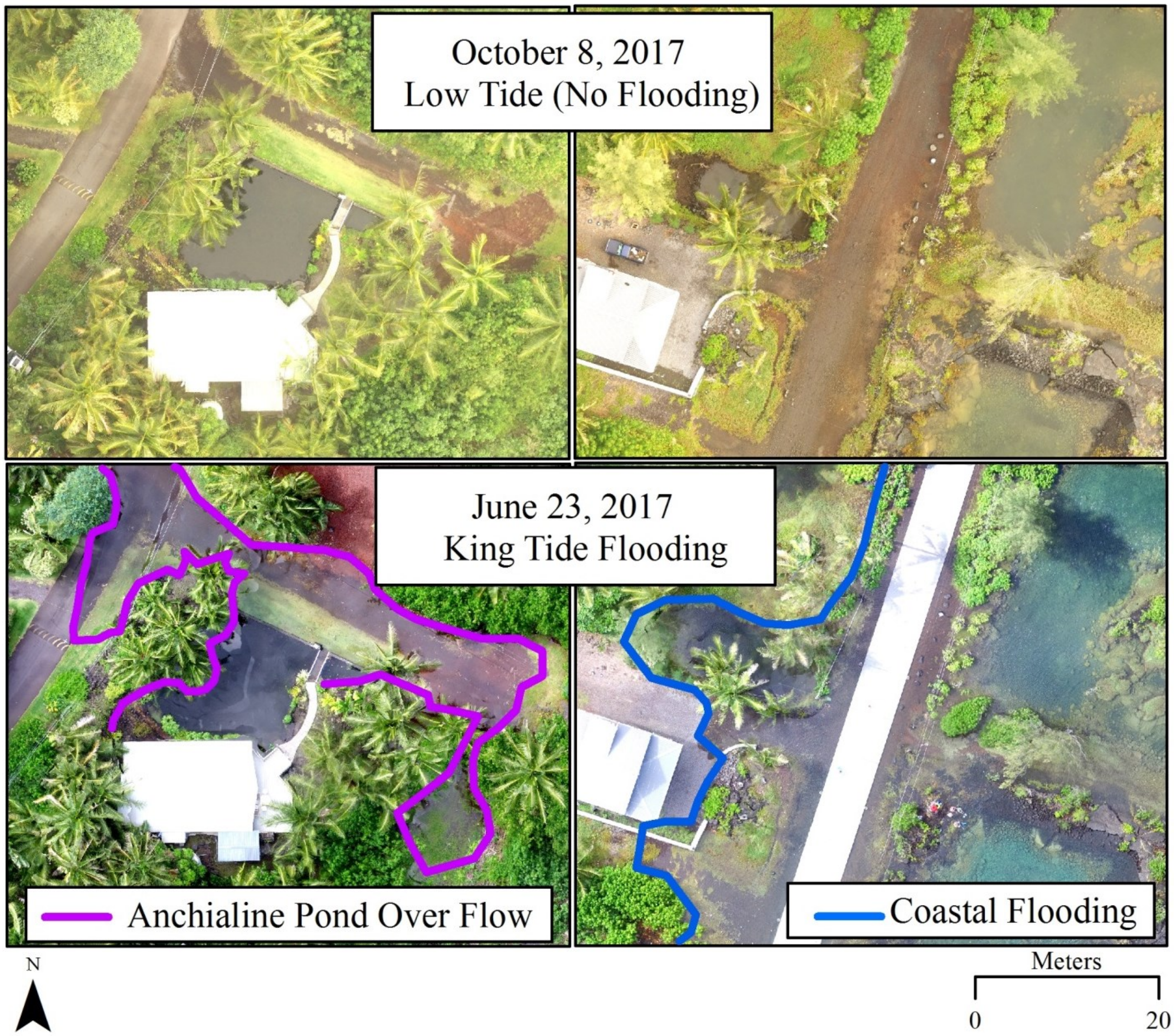

Figure 17. (Left) Delineation of flooded anchialine ponds; and (Right) delineation of direct coastal flooding. Top images are from the October 2017 low tide survey and bottom images are from the June 2017 king tide event.

4.2.3 Hydrostatic Modeling

In order to produce a hydrostatic model, we used similar methods described in section 2.2.5. Future water levels were determined by multiplying the sum of the SLR and the absolute value of the subsidence rate by pre-determined time intervals and adding the product to the MHHW (Table 9). We applied a SLR rate of 0.011 m yr^{-1} using the general estimate of nearly 1 meter of SLR by the year 2100 (Parris et al., 2012; Sweet et al., 2017; Hawai‘i Climate Change

Mitigation and Adaptation Commission, 2017). We use the maximum subsidence rate of -0.017 m yr^{-1} estimated by Hwang et al. (2007), which is important for informing more conservative, yet scientifically supported shoreline setbacks. We combined the maximum subsidence rate with the SLR rate at time intervals of 10, 25, 50, and 75 years. These time scales were collaboratively determined with input from the County of Hawaiʻi to represent the life expectancy of surrounding developments.

Table 9. SLR equations used to model SLR impacts in the future, where the variable *x* represents the time frame.

Time Frame	*Water Level Equation Used*
10 years	water level = 1.927 m + (0.011 m + 0.017 m)*x
25 years	water level = 1.927 m + (0.011 m + 0.017 m)*x
50 years	water level = 1.927 m + (0.011 m + 0.017 m)*x
75 years	water level = 1.927 m + (0.011 m + 0.017 m)*x

4.3 Results

4.3.1. Data Acquisition and Analysis

We were able to produce 0.02 m orthophotomosaics in Pix4D for the October and June 2017 surveys, which resulted in a RMSE of ± 0.07 m, and a June 2017 DSM with a vertical accuracy of ± 0.03 m. These errors are reported at the 95% confidence interval**.** We used both orthophotomosaics to identify existing anchialine ponds and delineate extreme flooding and pond overflow (Figure 18). Additionally, we use these data to show that present-day extreme flooding breaches the 20 ft setback, and in some areas supersedes the 40 ft setback line (Figure 18).

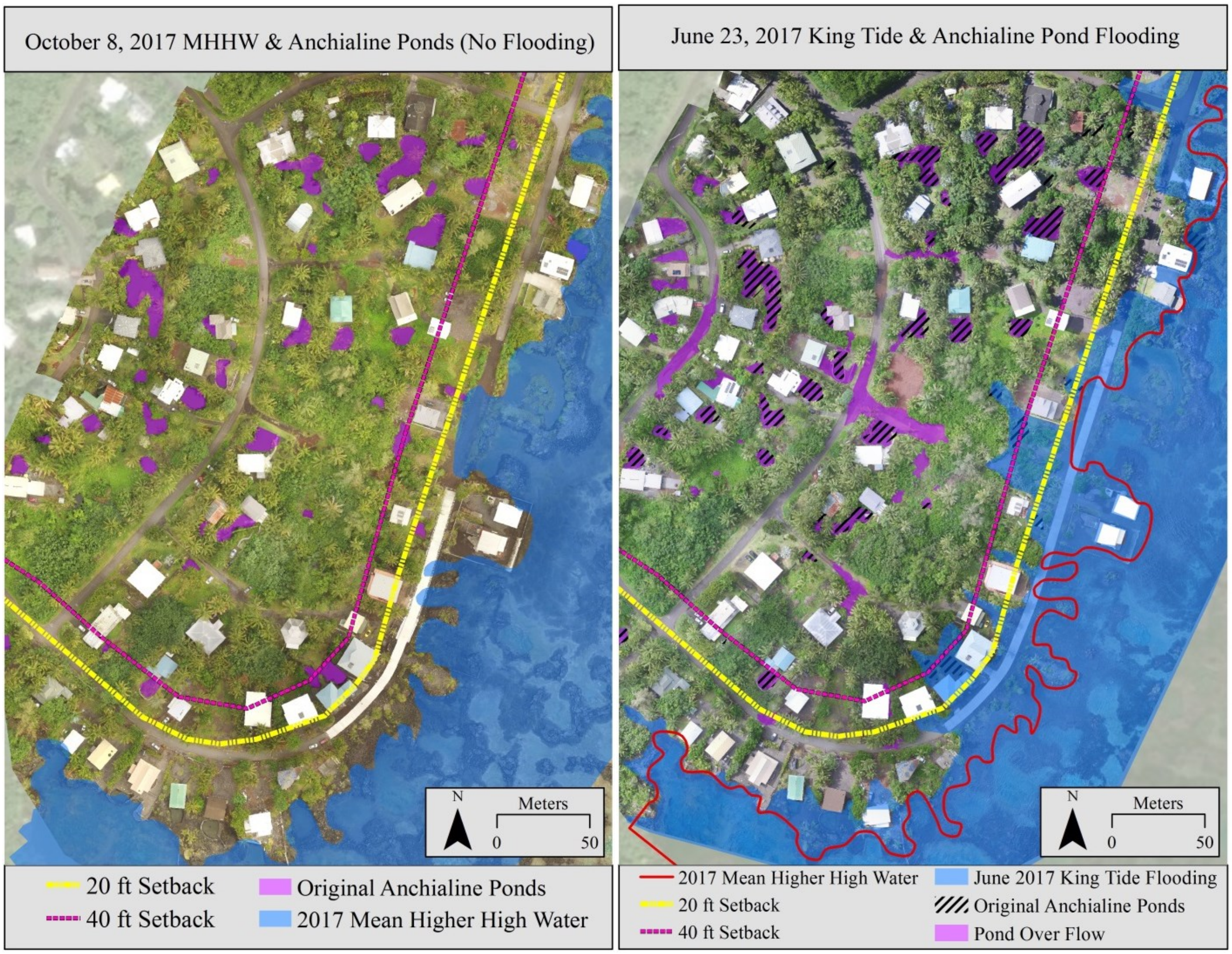

Figure 18. (Left) October 3, 2017 orthophotomosaic with anchialine ponds in dark purple and MHHW in dark blue; (Right) June 23, 2017 orthophotomosaic with anchialine pond over flow in dark purple, original anchialine pond boundaries in black dashes, extreme tide in dark blue, and MHHW delineated in red. The 20 ft and 40 ft setback are represented as the yellow and fuchsia dashed lines, respectively.

4.3.2. Hydrostatic Modeling

Based on our hydrostatic model, we expect that there could be nearly 2 m of SLR in 75 years. We estimate that in 10, 25, 50, and 75 years, the higher high water level will increase from 1.93 m to 2.21 m, 2.63 m, 3.32 m, and 4.03 m, respectively (Table 10) (Figure 19). Within 10 - 25 years, we see the entire study site is subject to flooding much greater than the June 2017 king tide event. At each projected time period, potential flooding completely supersedes the 20 ft and 40 ft setback boundaries (Figure 19).

Table 10. Description of water level, amount of TMKs, and amount of cesspools impacted at each time interval

Time	*Water Level*	*# TMK Affected*	*# OSWDS*
Present (King Tide)	0.945	97	39
SLR 10 years	2.207	122	63
SLR 25 years	2.627	130	65
SLR 50 years	3.327	140	80
SLR 75 years	4.027	143	88

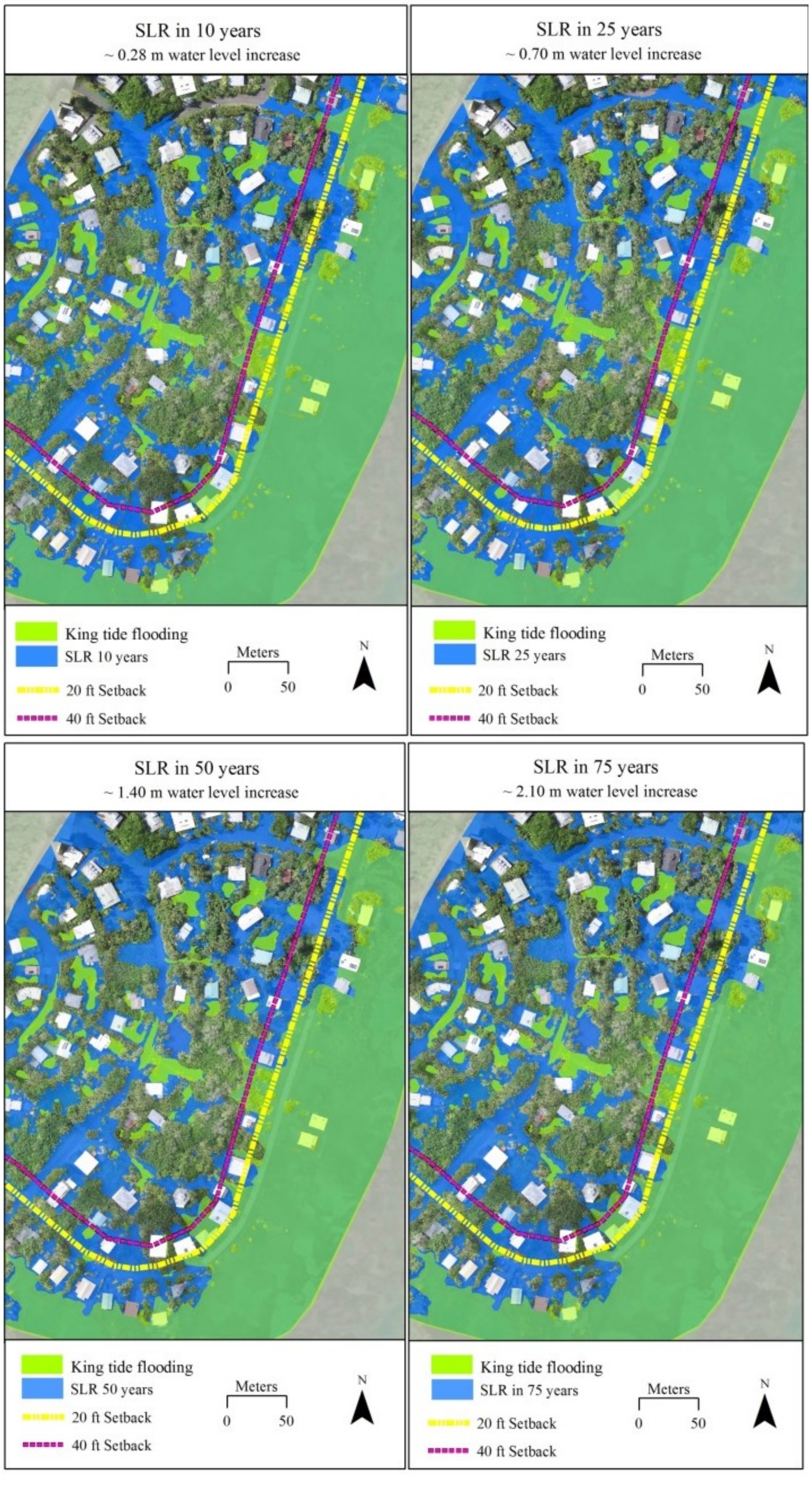

Figure 19. Potential flooding in 10, 25, 50, and 75 years. The June 2017 orthophotomosaic is used as a base map. The 20ft and 40 ft setbacks are identified as the yellow and fuchsia dashed lines, respectively. The bright green regions indicate flooding from the June 2017 king tide event.

4.3.3. Present and Future Impacts

We see that the June 2017 king tide event supersedes the 20 ft and 40 ft setback boundaries and causes inland flooding where there are anchialine ponds. We estimate that 97 out of 143 or 68% of total parcels/properties are impacted by any amount of present day extreme flooding (Figure 20) (Table 10). As a result, we estimate that 39 OSWDS might be flooded due to present-day tidal flooding and subsequent anchialine pond over flow (Figure 20) (Table 10).

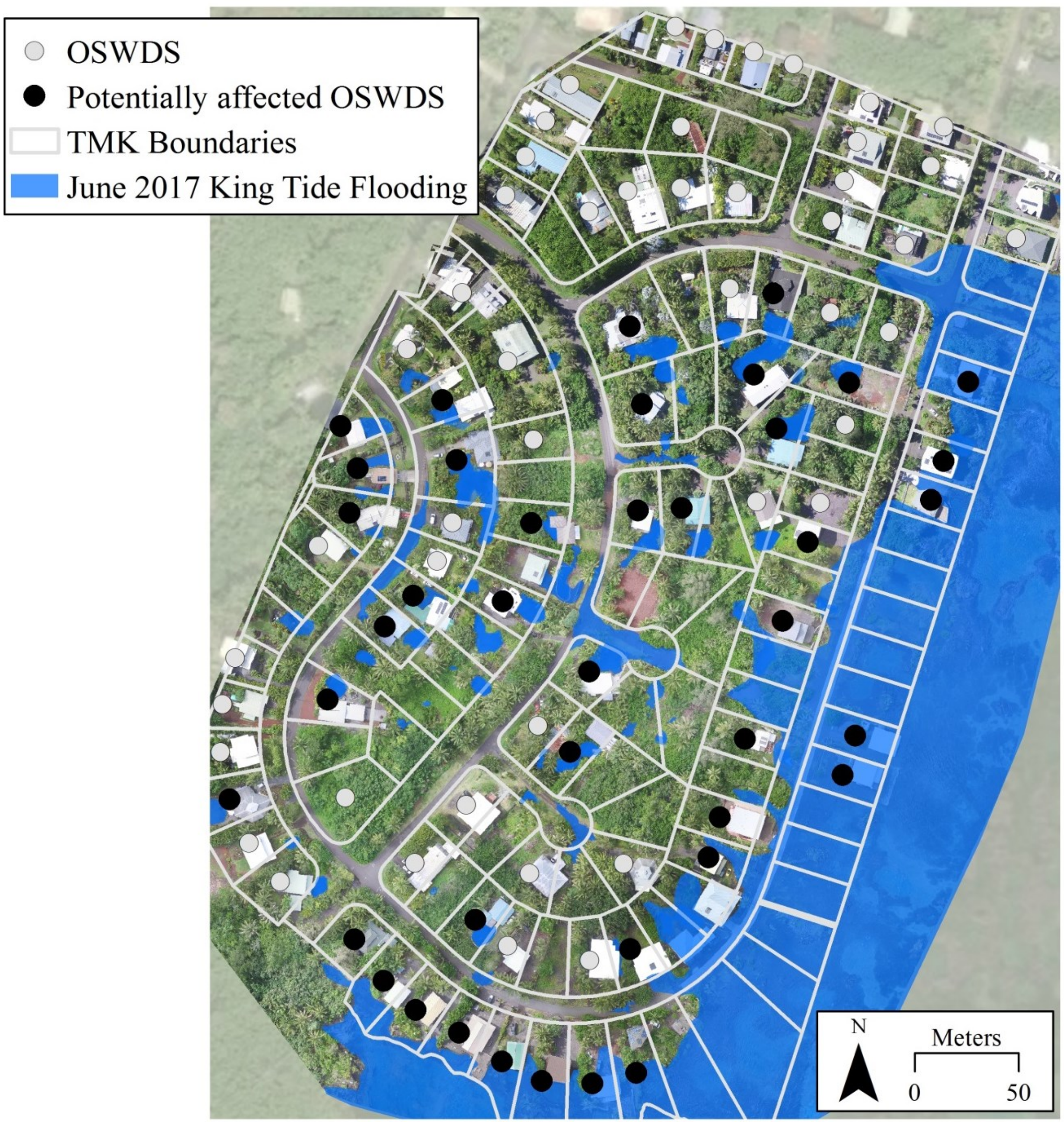

Figure 20. TMKs and possible onsite waste disposal systems impacted by the June 2017 king tide event

When we observe potential impacts from future SLR, we see that almost all parcels/properties experience flooding in as early as 25 years (Table 10). Within 50 years, we see that nearly all parcels/properties and cesspools will experience flooding (Table 10). Within 75 years, all parcels and cesspools will be affected by flooding (Table 9) (Figure 21).

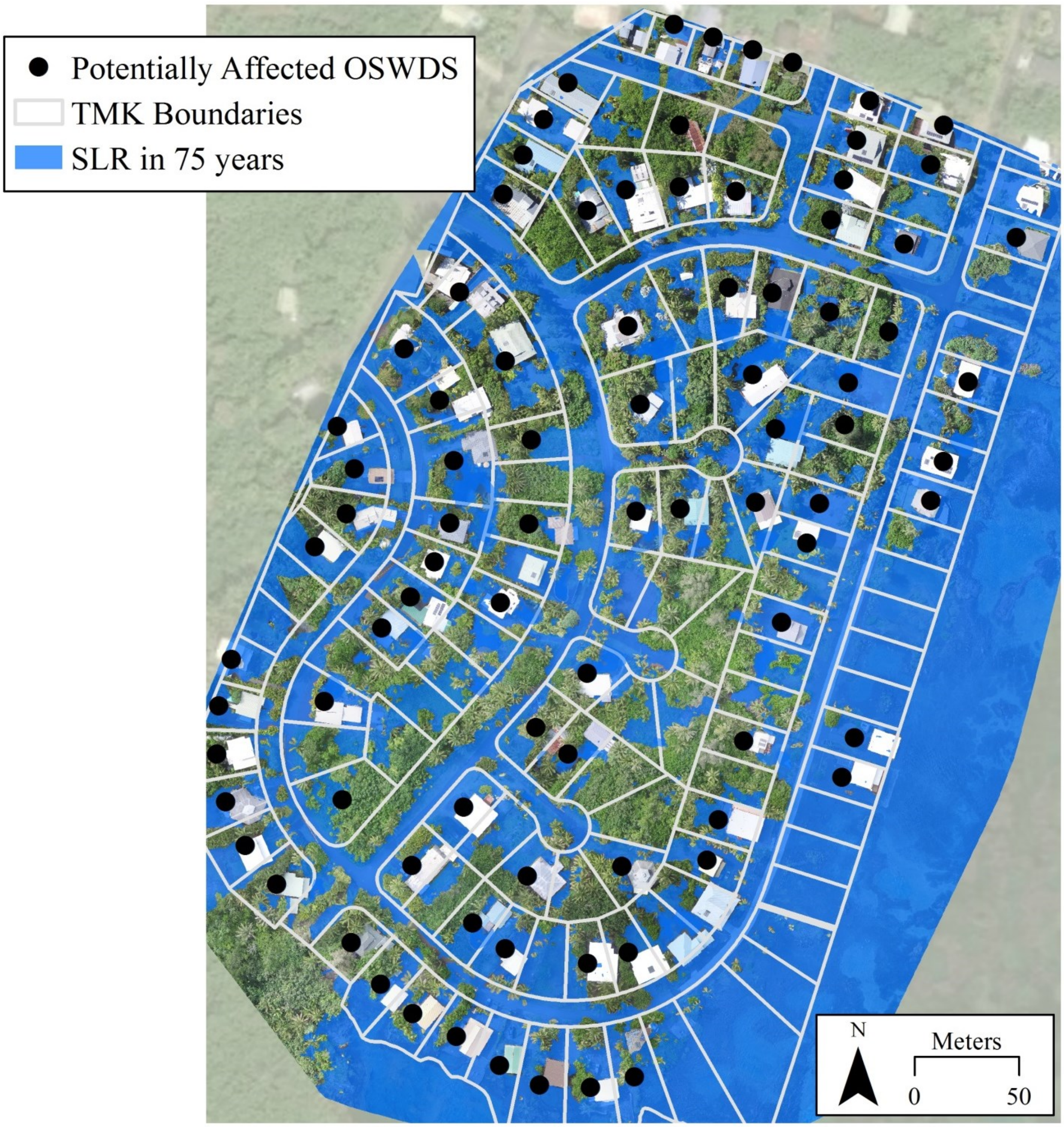

Figure 21. TMKs and onsite waste disposal systems impacted by SLR by 75 years

4.4 Discussion

We are able to use sUAS to rapidly collect data during an extreme high tide event and map the associated flooding within the Kapoho community. We further demonstrate that sUAS-acquired datasets are effective for producing elevation products that can be used for high resolution SLR modeling. We were able to further expand on hydrostatic SLR modeling approaches by incorporating subsidence rates with SLR rates for a place-based SLR assessment specific to the Kapoho community.

Our findings suggest that Kapoho is already seriously impacted by coastal hazards, evident by high tide nuisance flooding and extreme king tides. Nuisance flooding currently inhibits access and causes damage to certain properties, and completely submerges many of the OSWDS in the community. If our hydrostatic model is indicative of future SLR, this community will likely experience irreparable structural and ecological damage in the near future. Some properties are raised on cement stilts and therefore may be more resilient in the face of expected inundation. However, most of the inland properties are not raised and remain vulnerable to flooding. Additionally, there may be other ecological changes such as the emergence of new anchialine ponds (e.g. Marrack, 2015), an area of study that has not yet been explored along Hawaiʻi Island's eastern low-lying coastlines.

Based on our findings, we make three key recommendations: 1) elevation-based setbacks should be considered for low-lying and subsiding coastal environments; 2) Properties that have not been raised with stilts should consider mitigation strategies to prevent flooding damage; and 3) Onsite sewer disposal systems should be upgraded to prevent hazardous discharge into the nearby marine protected area. It is important to recognize that our results are derived from methods that assume subsidence and SLR conditions will remain constant into the future and thus do not consider flooding due to accelerated climate change scenarios, or worst-case subsidence/seismic events. Therefore, we also recommend that future studies research coastal vulnerabilities associated with accelerated SLR scenarios (e.g. Sweet et al., 2017) and occurrence of another significant subsidence event (e.g. Hwang et al., 2007).

Our methodologies could be applied to similar, vulnerable coastlines within Hawaiʻi and beyond. While some communities are already learning more about the combined impacts of SLR and subsidence (e.g. Marther et al., 2009), sUAS can be incorporated to map and monitor extreme flooding events that are expected to become the norm in the future. In doing so, homeowners, county planners, emergency responders, and engineers can better prepare for the future impacts of SLR.

4.5 Conclusion

We identify present and future coastal vulnerabilities to Kapoho, a low-lying and subsiding community on the east coast of Hawaiʻi Island. We see that extreme tides already flood certain properties and submerge OSWDS which cause hazardous nutrient and pathogen influx to the nearby marine protected area. Our hydrostatic model suggests that within 10 years the entire Kapoho community will experience flooding much greater than the June 2017 king tide event. We also confirm that 20 ft and 40 ft setback boundaries have not, and will not prevent hazardous development. Therefore it is necessary for homeowners, county planners, and engineers to take appropriate action to protect existing and future developments, and natural coastal resources. We recommend the consideration of elevation-based setbacks for Kapoho and similar communities, as well as the adoption of sUAS for rapid extreme tide or other nuisance flood mapping. In conclusion, this study allows us to learn from coastal hazards observed today to identify and prepare for future hazards.

CHAPTER 5: CONCLUSIONS

Coastal and island communities are becoming increasingly vulnerable to flooding from SLR and the exacerbated effects from coastal erosion and subsidence. As the global climate continues to rapidly change, impacts to these communities may be catastrophic and irreparable (Sweet et al., 2017; Hawaiʻi Climate Change Mitigation and Adaptation Commission, 2017). The state of Hawaiʻi in particular is vulnerable as its communities are already realizing the impacts of compounded coastal processes. This is due to Hawaiʻi being and island chain with most residents living on or near the coast. However, with careful planning and actionable science, some consequences may be reduced or even avoidable (Tribbia and Moser, 2008; Abbott, 2013). Based on our analyses at Hāpuna, Honoliʻi, and Kapoho, we offer three suggestions on how to implement relevant scientific data into place-based setbacks.

The approach described in Abbott (2013) can be directly used to establish appropriate setbacks along Hawaiʻi island's sandy beach coasts; the combination of historic aerial imagery analysis (e.g. Fletcher et al. 2003; Romine and Fletcher 2013) and short-term seasonal monitoring using sUAS can be used to determine shoreline change rates and applied to a place-based shoreline setback equation. Following Abbott (2013), this equation would add the designated shoreline setback distance to the product of the shoreline change rate and life expectancy of a structure (~50 – 100 yrs). For Hāpuna, the shoreline change rate applied could be the long-term erosion rate, or the short-term seasonal variation for a more aggressive setback policy. The equation for the former scenario could be as follows:

$$\textit{Hāpuna long-term setback} = 0.18\ m\ yr^{-1} * 50\ yrs + 12.19\ m = 21.19\ m\ (69.52\ ft) \tag{2}$$

For Hawaiʻi island's sea cliff environments, setbacks could be established two ways using the above equation 2 as a model. First, the setback could be based on a cliff edge shoreline and incorporate maximum cliff edge retreat (i.e. erosion episodes) to establish an aggressive shoreline setback, or long-term retreat to establish a conservative, yet still scientifically supported setback. In order for this to be effective, the cliff edge shoreline needs to be clearly defined so as to properly identify the shoreline in the first place (e.g. Hapke and Reid, 2007). Lastly, we recommend the consideration of elevation-based setbacks for Kapoho and similar low-lying coastal communities.

Our analyses using historic aerial imagery and sUAS-acquired imagery enabled us to produce the first dataset describing long- and short-term shoreline change rates specific to Hawaiʻi Island's diverse coast. Additionally, we applied sUAS to effectively monitor shoreline change on a temporal scale that has not been widely investigated. Our new understanding of past, present, and future changes at Hāpuna, Honoliʻi, and Kapoho has demonstrated that existing shoreline setbacks are not relevant across diverse geomorphic settings, and should be updated. Thus, we successfully produced data that can inform scientifically supported, place-based setbacks and other local coastal zone management strategies for Hawaiʻi County planners. We encourage other coastal and insular communities to apply and modify our methodologies to better understand their vulnerabilities, and join the collective effort to build resilient coasts.

REFERENCES

Abbott, T. 2013. Shifting shorelines and political winds - the complexities of implementing the simple idea of shoreline setbacks for oceanfront developments in Maui, Hawaiʻi. Ocean & Coastal Management. 73:13-21.

Anderson T., Fletcher C., Barbee M., Frazer M., and Romine B. 2015. Doubling of coastal erosion under rising sea level by mid-century in Hawaiʻi. Natural Hazards. 78: 75-103.

Barlow, J., Gilham, J., and Ibarra Cofrã, I. 2017. Kinematic analysis of sea cliff stability using UAV photogrammetry. International journal of remote sensing. 38(8-10): 2464-2479.

Barnard, P. L., Hoover, D., Hubbard, D. M., Snyder, A., Ludka, B. C., Allan, J., ... & McCandless, D. 2017. Extreme oceanographic forcing and coastal response due to the 2015–2016 El Niño. Nature Communications, *8* (14365).

Bode J. and Jol H. 2006. GPR investigation of Hapuna Beach, Hawaiʻi: Coastal and fluvial deposits. Proceedings of the Eleventh International Conference on Ground Penetrating Radar.

Brooks B., Merrifield M., Foster J., Werner C., Gomez M., and Gill S. 2007. Space geodetic determination of spatial variability in relative sea level change, Los Angeles basin. Geophysical Research Letters. 34: L01611.

Brown, J. M., Phelps, J. J., Barkwith, A., Hurst, M. D., Ellis, M. A., and Plater, A. J. 2016. The effectiveness of beach mega-nourishment, assessed over three management epochs. Journal of environmental management. 184: 400-408.

Casella1 E., Rovere A., Pedroncini A., Stark C., Casellao M., Ferrari M., and Firpo M. 2016. Drones as tools for monitoring beach topography changes in the Ligurian Sea (NW Mediterranean). Geo-Marine Letters. 19: 831–845.

Conrad C. 2013. The solid Earth’s influence on sea level. Geological Society of America. 125: 1027-1052.

Council of the County of Kauai. 2014. The Comprehensive Zoning Ordinance code 1987. County of Kauai. Chapter 8.

Crowell M., Leatherman S., Buckley, M. 1993. Shoreline change rate analysis: long term versus short term data. Shore and Beach. 16:13-20.

Dewez, T. B., Leroux, J., and Morelli, S. 2016. Cliff collapse hazard from repeated multicopter UAV acquisitions: return on experience. The International Archives of Photogrammetry, Remote Sensing and Spatial Information Sciences. 41: 805-811.

Dickson, M. E., Walkden, M. J., and Hall, J. W. 2007. Systemic impacts of climate change on an eroding coastal region over the twenty-first century. Climatic Change. 84(2): 141-166.

Dow J.M., Neilan R.E., and Rizos C. 2009. The International GNSS Service in a changing landscape of Global Navigation Satellite Systems. Journal of Geodesy. 83: 191–198.

Dugan, J. E., Defeo, O., Jaramillo, E., Jones, A. R., Lastra, M., Nel, R., ... and Schoeman, D. S. 2010. Give beach ecosystems their day in the sun. Science. 329(5996): 1146-1146.

Emery, K.O. and Kuhn G.G. 1982. Sea cliffs: their processes, profiles and classification. Geological Society of America Bulletin. 93: 644–654.

Fletcher C., Grossman E., Richmond B., and Gibbs A. 2002. Atlas of natural hazards in the Hawaiian coastal zone. U.S. Geologic Survey Geologic Investigations Series I-2761. 129-181.

Fletcher C., Rooney J., Barbee M., Lim S., and Richmond B. 2003. Mapping shoreline change using digital orthophotogrammetry on Maui, Hawaiʻi. Journal of Coastal Research. 38: 106-124

Ford M. 2013. Shoreline changes interpreted from multi-temporal aerial photographs and high resolution satellite images: Wjote Atoll, Marshall Islands. Remote Sensing of Environment. (135)130-140.

Gallop S., Bosserelle C., Haigh I., Wadey M., Pattiaratchi C., and Eliot I. 2015. The impact of temperate reefs on 34 years of shoreline and vegetation line stability at Yanchep, southwestern Australia and implications for coastal setback. Marine Geology. 369: 224-232.

Galloway, D. L., Jones, D. R., and Ingebritsen, S. E. 1999. Land subsidence in the United States Vol. 1182. US Geological Survey.

Goncalves J. and Henriquez R. 2015. UAV photogrammetry for topographic monitoring of coastal areas. Journal of Photogrammetry and Remote Sensing. 104: 101-111.

Habel S., Fletcher C., Barbee M., and Anderson T. 2017. The influence of seasonal patterns on a beach nourishment project in a complex reef environment. Coastal Engineering. 116: 67-76.

Haer, T., Kalnay, E., Kearney, M., and Moll, H. 2013. Relative sea-level rise and the conterminous United States: Consequences of potential land inundation in terms of population at risk and GDP loss. Global Environmental Change. 23(6): 1627-1636.

Hapke C., and Reid D. 2007. National assessment of shoreline change, part 4: historical coastal cliff retreat along the California Coast: U.S. Geological Survey open-file report. USGS. 2007-1133.

Houston, J. R. 2008. The economic value of beaches: a 2008 update. Shore and beach, 76(3): 22-26.

Hurst, M. D., Rood, D. H., Ellis, M. A., Anderson, R. S., & Dornbusch, U. 2016. Recent acceleration in coastal cliff retreat rates on the south coast of Great Britain. Proceedings of the National Academy of Sciences. 113(47): 13336-13341.

Hwang D. 2007. Coastal subsidence in Kapoho, Puna, island and state of Hawaiʻi. Hawaiʻi County Planning Department. 5-18.

Johnson, J. 2002. Establishing Development Setbacks from Coastal Bluffs. Proceedings, California and the World Ocean. n. pag. Orville Magoon. Web.

Johnstone, E., Raymond, J., Olsen, M. J., and Driscoll, N. 2016. Morphological expressions of coastal cliff erosion processes in San Diego County. Journal of Coastal Research, 76(1): 174-184.

Knopp G. and Scheffler T. 2016. Coastal erosion study: Meurer property Opihikao, Puna District, Island of Hawaiʻi. Geohazards Consultants International, Inc.

Landry, C. E., Keeler, A. G., and Kriesel, W. 2003. An economic evaluation of beach erosion management alternatives. Marine Resource Economics. 18(2): 105-127.

Leshchinsky, B., Olsen, M. J., Mohney, C., Glover-Cutter, K., Crook, G., Allan, J., ... & Mathews, N. 2017. Mitigating coastal landslide damage. Science. *357*(6355): 981-982.

Lim, M. and Petley, D. N. and Rosser, N. J. and Allison, R. J. and Long, A. J. and Pybus, D. .2005. Combined digital photogrammetry and time-of-flight laser scanning for monitoring cliff evolution. Photogrammetric record. 20 (110): 109-129.

Makai Ocean Engineering Inc. and Sea Engineering Inc. 1991. Aerial photography analysis of coastal erosion on the islands of Kauaʻi, Molokaʻi, Lānaʻi, Maui, and Hawaiʻi. State of Hawaiʻi Office of State Planning Zoastal Zone Management Program.

Marrack L., 2015. Incorporating groundwater levels into sea-level detection models for Hawaiian anchialine pool ecosystems. Journal of Coastal Research. 31(5): 1170–1182.

Marther A., Garland G., and Stretch D. 2009. Southern African sea levels: corrections, influences and trends. African Journal of Marine Science. 31(2): 145-156.

Maui Planning Commission. 2007. Shoreline rules for the Maui Planning Commission. Department of Planning. Chapter 203.

Moftakhari, H. R., A. AghaKouchak, B. F. Sanders, D. L. Feldman, W. Sweet, R. A. Matthew, and A. Luke. 2015. Increased nuisance flooding along the coasts of the United States due to sea level rise: past and future, Geophysical Research Letters. 42: 9846–9852. doi:10.1002/ 2015GL066072.

Neumann J., Vafeidis A., Zimmerman J., and Nicholls R. 2015. Future coastal population growth and exposure to sea-level rise and coastal flooding - a global assessment. PLOS ONE 10(6): e0131375. (A)

Neumann J. Emanuel K., Ravela S., Ludwig L., Kirshen P., Bosma K., and Martinish J. 2015. Joint effects of storm surge and sea-level rise on US Coasts: new economic estimates of impacts, adaptation, and benefits of mitigation policy. Climate Change. 129: 337-349. (B)

Parham J., Higashi G., Lapp E., Kuamoʻo D., Nishimoto R., Hau S., Fitzsimons M., Polhemus D., and Devick W. 2008. Atlas of Hawaiian watersheds and their aquatic resources.

Division of Aquatic Resources and Bishop Museum. http://www.Hawai‘iwatershedatlas.com/authors.html

Parris, A., P. Bromirski, V. Burkett, D. Cayan, M. Culver, J. Hall, R. Horton, K. Knuuti, R. Moss, J. Obeysekera, A. Sallenger, and J. Weiss. 2012. Global Sea Level Rise Scenarios for the US National Climate Assessment. NOAA Tech Memo OAR CPO-1. 37 pp.Quan, S., Kvitek, R., Smith, D., and Griggs, G. 2013. Using vessel-based LIDAR to quantify coastal erosion during El Niño and inter-El Niño periods in Monterey Bay, California. ˜ Journal of Coastal Research. 29(3): 555–565.

Romine B., Fletcher C., Frazer L., Genz A., Barbee M., and Lim S. 2009. Historical shoreline change, Southeast Oahu, Hawai‘i: applying polynomial models to calculate shoreline change rates. Journal of Coastal Research. 25(6): 1236–1253.

Romine B. and Fletcher C. 2013. A Summary of Historical Shoreline Changes on Beaches of Kauai, Oahu, and Maui, Hawai‘i. Journal of Coastal Research. 29(3): 605-14.

Stephenson, N., Perroy, R., Eiben, J., & Klasner, F. 2017. High resolution habitat suitability modelling for an endemic restricted-range Hawaiian insect (Nysius wekiuicola, Hemiptera: Lygaeidae). Journal of Insect Conservation. 21(1): 87-96.

Sweet W., Kopp R., Weaver C., Obeysekera J., Horton R., Thieler E., and Zervas C. 2017. Global and regional sea level rise scenarios for the United States. NOAA Technical Report NOS-OPS 083.

Thieler E., Himmelstoss E., Zichichi J., and Ergul A. 2009. Digital Shoreline Analysis System (DSAS) version 4.0—An ArcGIS extension for calculating shoreline change: U.S. Geological Survey Open-File Report.

Tribbia, J., & Moser, S. C. 2008. More than information: what coastal managers need to plan for climate change. Environmental science & policy.11(4): 315-328.

Turner I., Harley M., and Drummond C. 2016. UAVs for Coastal Surveying. Coastal Engineering. 114: 19-24.

Vitousek, S., Barbee, M. M., Fletcher, C. H., Richmond, B. M., & Genz, A. S. 2009. Pu’ukohola–Heiau National Historic Site and Kaloko-Honoko–hau Historical Park, Big Island of Hawai’i. Coastal Hazard Analysis Report. NPS Geologic Resources Division, Honolulu, HI.

Warrick J., Ritchie A.; Adelman G., Adelman K., and Limber P., 2017. New techniques to measure cliff change from historical oblique aerial photographs and Structure-from-Motion photogrammetry. Journal of Coastal Research. 33(1): 39–55.

Yoo C. and Oh T. 2016. Beach volume change using UAV photogrammetry Songjung Beach, Korea. The International Archives of the Photogrammetry, Remote Sensing and Spatial Information Sciences. XLI-B8: 1201-1205.

Young, A. P. 2018. Decadal-scale coastal cliff retreat in southern and central California. Geomorphology. *300*: 164-175.